

Confidential



Forest Industry Applications of UAVs

Grant Pearse, Michael Watt



Report information sheet

Report title	Industry Application of UAVs
Authors	Grant Pearse, Michael Watt
Client	FOA
Client contract number	A63406
MBIE contract number	If applicable
SIDNEY output number	58999
Signed off by	Michael Watt
Date	June 2017
Confidentiality requirement	Confidential (for client use only)
Intellectual property	© New Zealand Forest Research Institute Limited. All rights reserved. Unless permitted by contract or law, no part of this work may be reproduced, stored or copied in any form or by any means without the express permission of the New Zealand Forest Research Institute Limited (trading as Scion).
Disclaimer	<p>The information and opinions provided in the Report have been prepared for the Client and its specified purposes. Accordingly, any person other than the Client uses the information and opinions in this report entirely at its own risk. The Report has been provided in good faith and on the basis that reasonable endeavours have been made to be accurate and not misleading and to exercise reasonable care, skill and judgment in providing such information and opinions.</p> <p>Neither Scion, nor any of its employees, officers, contractors, agents or other persons acting on its behalf or under its control accepts any responsibility or liability in respect of any information or opinions provided in this Report.</p>

Executive Summary

Remotely sensed data are widely used in the forestry sector. These data have largely been sourced from satellite or airborne sensors. Recently, unmanned aerial vehicles (UAVs) have emerged as a new platform for acquiring remotely sensed data. In contrast to satellites and aircraft, UAVs are relatively inexpensive and can be rapidly deployed to collect data with high frequency. These craft have restricted flight times and payload capacity, limiting the potential range of applications and the type of sensors that can be carried. These attributes are likely to see UAVs fill a niche for the collection of remote sensing data to serve a variety of novel applications. This report presents findings from a study conducted by Scion investigating the roles and cost efficacy of UAVs for data collection as well as four potential applications highlighted by the forest industry. The applications for UAV imagery investigated were: 1) identification and mapping of wind-damaged forest to plan for value recovery; 2) identification and mapping of cutover areas; 3) assessment of post-planting stocking and survival; 4) post-harvest waste assessment.

A survey of commercial providers was conducted to contrast costs for airborne, satellite, and UAV remote sensing data. Aircraft was the only practical and cost-effective means of collecting LiDAR data for forestry. Costs were strongly impacted by the area and pulse density required, with prices varying from \$2-5/ha for large, low-density campaigns up to \$15-20/ha for small or specialist campaigns. Satellites were the most cost effective for imagery, providing 100 ha for as little as \$1.50; however, large minimum order areas and the coarse spatial resolution limited the range of applications for these data. Aerial imagery with higher spatial resolution cost from \$10-20/ha but also required minimum areas and both platforms could require significant delays between order and collection. UAVs offered acquisition of RGB and multispectral data with very high spatial and temporal resolution. Prices varied significantly depending on the data, craft, and processing required. Fixed wing craft could capture RGB imagery for \$3-10/ha over areas of up to 100 ha or even 2000 ha for some larger fixed-wing craft. Multirotors offered very high resolution imagery, easy deployment, and moderate payload capacity at the expense of range. UAVs had no minimum order area and could be deployed within hours to capture data. Basic craft and sensors could be purchased and operated for under \$5000 or crews and craft could be hired for a fixed rate of \$2500-\$3000 per day. UAVs serve a niche for rapid and cost-effective collection of imagery over small to moderate areas using less-sophisticated sensors.

Wind damage is a major risk to planted and natural forests in New Zealand and effective mapping and planning can assist with damage assessment and value recovery. A fixed wing UAV was used to collect RGB imagery over a wind-damaged forest in the Nelson region. These data could be accurately classified into affected / unaffected areas using simple methods such as Mahalanobis classification. This approach produced similar estimates to manual mapping (10.8 ha cf. 9 ha). The process correctly identified wind-damaged areas missed during manual mapping and provided finer detail for updating stand records. Overall, UAV imagery appeared useful for rapid assessment of post-storm wind damage in forests. A multirotor craft provided much higher resolution RGB imagery to test stem detection over the same site. An object-based image analysis performed on a filtered and transformed version of the scene was largely successful in delineating stems on the ground and appeared to show promise for obtaining stem counts with further refinements.

Cutover assessment is important for monitoring progress during harvest operations and for updating stand records after harvesting is complete. A series of images showing forested and recently harvested areas were used to develop methods for detecting the boundary between forest and cutover. A computationally simple colour space transformation provided mean classification accuracy of 83.2%; however, more complex classification using support vector machines provided superior accuracy of 90.2%. The edge-detection and tracking algorithm showed a mean deviation of 2.4 m from the actual boundary when applied to pre-recorded test data. A collaborative project with the University of Canterbury led to the development of an

affordable custom UAV equipped with a video camera and programmable navigation system. The UAV was successfully programmed to apply the edge-detection algorithm in real-time to detect and follow the edge of a recently harvested site in Canterbury. The results showed that imagery from inexpensive UAVs could be used to accurately map forest cutover and the UAV system developed showed potential for regular, automated updating of the cutover boundary using inexpensive UAVs.

Post-planting assessment is important to ensure initial planting has reached the target stocking and to assess survival in order to fill areas with high mortality during the next planting season. RGB imagery was acquired at a test site to trial a range of methods for counting seedlings younger than 1 year. Object-based approaches using the spectral properties of seedlings in combination with contrast features had a precision of 83% and sensitivity of 86%. A method based on the normalised cross-correlation coefficient between image windows and a template derived from a large training sample improved on these results. The method had a sensitivity of 89% while the precision of the classifier was 92%. Both methods used only RGB data, but the addition of multispectral data from higher-resolution sensors is likely to significantly improve these approaches.

Post-harvest waste assessment is traditionally conducted using the line intersect method (LIM) to compute a residual volume of timber left unrecovered on the site. RGB imagery from a UAV was acquired over a recently harvested area and used to develop a very high resolution orthomosaic. Measurements obtained using traditional ground-based LIM methods and digitised measurements obtained from the UAV imagery were compared. The length, intercept diameter, and large and small end diameters all showed strong agreement. Measuring length using imagery produced the highest error (mean difference of 9.9 cm). Volumes calculated from the field and image-based measurements agreed strongly ($R^2 = 0.95$) with a mean difference of 0.02 m³. Traditional LIM methods computed using the cross-sectional diameters extracted from the field and image-based measurement of pieces along 16 transects showed strong agreement. Overall, UAV-derived imagery appeared well suited to the estimation of post-harvest waste volumes. Further testing and development may validate several apparent advantages offered by this approach.

Overall, the results from this study showed that UAVs fill a niche in terms of remote sensing data that is not currently served by other platforms. As such, UAVs are likely to complement rather than replace traditional remote sensing methods. The results from this study showed UAV imagery to be useful at the proof of concept level for all of the potential applications highlighted for investigation. The rapid development of methods, craft, and sensors are likely to see greatly expanded uses for UAVs within the forest industry in the future.

Industry Applications of UAVs

Table of contents

Executive Summary.....	3
Table of contents	5
Introduction and Overview	6
Roles and Cost Efficacy of UAVs	7
Background.....	7
Satellite imagery	8
Airborne sensors	8
Unmanned aerial vehicles	10
Conclusions	14
Wind Damage Assessment.....	15
Background.....	15
Data and methods	16
Results.....	18
Discussion and conclusions	22
Automated Cutover Detection	23
Background.....	23
Methods	24
Results.....	27
Discussion and conclusions	29
Post-planting assessment	30
Background.....	30
Methods	31
Results.....	35
Discussion and conclusions	37
Post-harvest Waste Assessment.....	38
Background.....	38
Methods	39
Results.....	41
Discussion and conclusions	43
Conclusions	44
Acknowledgements.....	45
References.....	46

Introduction and Overview

Remote sensing is widely used in the management of both natural and planted forests for a range of applications (Holmgren & Thuresson, 1998; J. C. White et al., 2016). In New Zealand, many companies use remote sensing for tasks ranging from mapping and health assessment using imagery to inventory and harvest planning using LiDAR (Morgenroth & Visser, 2013). These applications traditionally rely on remotely sensed data from aircraft and satellite platforms. The sensors carried by these platforms are often expensive, sophisticated, and tasked on-demand with the costs of data acquisition often reflecting these facts. Recently, unmanned aerial vehicles have emerged as a new platform for data acquisition. These craft are often inexpensive and many can only carry light payloads for a limited time. However, the low cost and capability for rapid deployment mean that UAVs are increasingly being used across a range of disciplines (Grenzdörffer, Engel, & Teichert, 2008; Pajares, 2015; Wallace, Musk, & Lucieer, 2014). Scion has been running a UAV research programme exploring a wide range of applications for UAVs. This report examines the cost efficacy and potential roles that UAVs might play within the forestry sector. Proof of concept studies were conducted to address four potential applications for UAVs highlighted by the forestry sector and Scion researchers. These include: 1) identification and mapping of wind-damaged forest to plan for value recovery; 2) identification and mapping of cutover areas; 3) assessment of post-planting stocking and survival; 4) post-harvest waste assessment. The studies were wide-ranging and focused primarily on assessing the practicality and potential for UAV-acquired data to assist with the highlighted applications. The studies also deliberately included the use of a wide range of UAVs, sensors, image analysis tools, and different forest types to reflect the varied roles and environments these platforms are likely to operate in across the forestry sector.

Roles and Cost Efficacy of UAVs

Background

Forest management in New Zealand makes extensive use of remotely sensed data, with high-resolution aerial imagery for mapping activities being the leading application for many forest companies (Morgenroth & Visser, 2013). Airborne laser scanning (ALS or LiDAR) has also been adopted for an increasingly broad range of applications such as forest inventory. However, the key use of LiDAR for many companies remains the ability to extract a high-resolution digital terrain model (DTM) below the canopy for use in harvest planning and engineering. Satellite imagery has seen less uptake; however, some companies have found applications for the increased spectral resolution available from modern sensors in assessments of health and disturbance (Morgenroth & Visser, 2013).

Until recently, remotely sensed data for forestry was nearly exclusively acquired from aircraft, primarily fixed wing aeroplanes with occasional use of helicopters for some tasks. In the last 30 years, satellites have also played an increasingly important role but offer limited spatial resolution. More recently, UAVs have emerged as a new source of remotely sensed data. The technological capabilities of these craft now allow a range of sensors to be flown along precise pre-determined flight paths. These craft are typically much smaller than fixed wing aeroplanes or helicopters and can fly at considerably lower altitudes. The cost of these craft has also decreased and both fixed wing and multirotor models typically require much less preparation and planning and can be launched and landed in much smaller areas. The usefulness of aerial RGB imagery within forestry is of particular interest with regards to UAVs as these craft have evolved with RGB capture as a fundamental capability.

The flexibility of UAVs and the provision of key products such as RGB and multispectral data would appear to make UAVs well suited to a range of forestry-related remote sensing tasks. However, UAV technology has practical and technical limitations that restrict the range of tasks that these platforms are suited to in the forestry context. For example, most civilian craft are severely limited in terms of the sensor payload they can accommodate and regulatory restrictions and uncertainty further constrain the range of potential applications.

As part of this research report, a survey of satellite, aerial, and UAV suppliers was conducted. The purpose of this survey was to identify and compare costs, services, and operational considerations for each of these platforms, especially in terms of applications within the forestry sector. A range of suppliers from New Zealand and Australia were surveyed to collect these data. Providers ranged from general contract providers covering many industries to highly specialised operators providing niche services to the forestry sector. Businesses ranged in scale from individual operators with a small number of UAVs to larger organisations with several fixed wing aircraft. Telephone interviews were wide-ranging but all conversations covered the costs, platform constraints and advantages, and primary uses within forestry. Many respondents preferred cost information to remain anonymous. To accommodate this, cost information (excluding satellite data) was pooled and converted to indicative bands. In every case, providers indicated a high variance in prices, with actual costs depending strongly on factors such as location, weather, job size, service level, and many other factors. Therefore, costs can only be considered as indicative and are intended only as a general guideline to compare cost efficacy of different platforms.

Satellite imagery

A recent survey indicated limited use of satellite imagery in the New Zealand forestry sector, with companies usually acquiring these data for input into a GIS as part of mapping activities (Morgenroth & Visser, 2013). Cost data for satellite imagery are shown in Table 1. Spatial resolution was the primary determinant of cost, with other factors such as spectral resolution (number of bands) and acquisition timeframe also impacting the pricing. A key factor to be considered for forestry applications is the acceptable level of cloud cover and requirements for a minimum area to be purchased. For WorldView 3, which has one of the highest spectral and spatial resolutions commercially available, the minimum purchase is 100 km² (10,000 ha) meaning a minimum cost of NZ\$4,700 for this imagery. The acceptable age of the imagery can impact costs as well. Archive imagery older than 90 days is typically discounted by ~ 35%. However, the availability of this imagery is dependent on the satellite having acquired it as part of a previous tasking. Urgent imagery collected within a timeframe of weeks, for example, imagery urgently ordered to assess wind-throw damage, may be up to 60% more expensive than imagery from more typical acquisition windows of 30 – 45 days.

Table 1: Indicative prices for different satellite imagery products. Costs may also vary for archive imagery, reduced cloud cover, and urgent acquisitions.

Satellite	Resolution	Bands	Cost (per km ²)	Minimum Order (tasked)
RapidEye	5 m	5	\$1.50	3500 km ²
SPOT 6, 7/Azersky	5 m	4	\$1.70	500 km ²
SPOT 6, 7/Azersky	1.5 m	4	\$4	500 km ²
Kompsat	0.50 m	4	\$17	100 km ²
Pléiades	0.50 m	4	\$30	100 km ²
WorldView-3	0.30 m	4/8	\$47	100 km ²

The satellite earth observation sector is rapidly changing. After many years of moderate growth in the constellation size and gradual reductions in cost, a large number of new entrants have announced funded constellations of moderate to high-resolution satellites. These changes have been spurred on by well-publicised advances in orbital launch capabilities such as Ariane 5 (EU) reaching 74 consecutive launch successes, and the arrival of lower-cost launch vehicles such as PSLV (India), SpaceX Falcon 9 (USA) and Orbital ATK Minotaur & Antares (US). In total, new constellations such as SkySat (13-25), BlackSky (60), and Terra Bella / Planet (24 + 200) will bring the total number of earth imaging satellites to over 200 by 2020, potentially increasing availability and reducing costs for image acquisition. Cheaper sensors may sacrifice spatial resolution and geometric accuracy to provide very high revisit times. This may limit practical applications of some platforms to broad-scale change detection using a small set of bands e.g. RGB + Near Infrared (NIR).

Globally, space-borne sensors have partially replaced aircraft imagery as a major source of remote sensing data. Satellite programs such as Landsat and IKONOS have captured millions of square kilometres worth of imagery, which would have previously been impossible to acquire from aircraft. US restrictions on satellite imagery resolution have recently been eased, enabling the resale of much higher resolution products (0.3 m from WorldView3). Although these new products can in many instances match aircraft sensors of a few years ago, aircraft sensors such as the Ultracam (Vexcel Imaging, Graz, Austria) have advanced at a similar pace and offer their own combination of advantages relative to satellite sensors (Toth & Józków, 2016).

Airborne sensors

Aircraft have a long lineage as platforms for forestry related remote sensing data acquisition. As a platform, aircraft offer an appealing combination of reduced lower altitude

flight capability (reduced atmospheric interference); large, flexible payload capacity and capability to survey very large areas with high resolution (Toth & Józków, 2016). Aerial imagery is the most commonly used source of remote sensing data for New Zealand forest managers, with 88% of surveyed companies making regular use of RGB aerial imagery (Morgenroth & Visser, 2013).

Aerial service providers surveyed for this report indicated forest management companies as significant customers across most parts of New Zealand. Although imagery remained an important product for the industry, LiDAR data acquisition was close to or over 50% of the contracted work for all larger respondents with the capability to acquire these data. Multispectral imagery was routinely captured (NIRGB), and one provider was exploring the use of forest health assessment services based on analysis of hyperspectral data. Costs for aerial imagery and LiDAR varied according to a number of factors such as distance to the forest, the size of the surveyed area, final product specifications (e.g. pulse density for LiDAR, ground sample distance (GSD) for imagery), and external factors such as weather. Table 2 provides indicative costs for acquisition of aerial imagery and LiDAR.

Table 2: Indicative costs for imagery and LiDAR acquired from aircraft.

Aerial data product	Minimum area (ha)	\$ / ha @ minimum area	Maximum area (ha)	\$ / ha @ maximum area
Imagery	100 - 500	\$10 - 20	No limit	\$<1 - 3
LiDAR	500	\$15 - 20	No limit	\$2 - 5

Aircraft operators indicated no upper limit to the potential area for LiDAR or aerial imagery. Although satellite platforms can theoretically capture planet-wide data, for all practical forestry-related tasks aircraft can be considered to have equivalent capabilities in terms of scale. While cloud cover and illumination may restrict satellite image capture, aircraft are somewhat more flexible. The majority of providers surveyed operated across several regions, allowing flexible deployment of aircraft to suit local weather conditions. In many cases, aircraft could be redeployed and collecting imagery within 1-3 days. Despite this advantage, solar illumination during winter was noted by all providers as an obstacle to image acquisition. A small number of suitable hours available per day for this work reduced the scale advantage of aircraft operation but data could still be collected at higher rates per hectare. LiDAR acquisition was noted to be sensitive to a range of weather factors with precipitation, snow cover, mist or fog, and high winds all posing challenges to acquisition and data quality.

A key finding from the survey results was that aerial data acquisition often represented a smaller portion of the costs than data processing. Minimum specifications for accuracy, pulse density, geolocation precision, and other factors meant that, for both imagery and LiDAR, acquisition represented 50% or less of the total costs. Imagery was observed to require considerable post-processing for image registration, orthorectification, and georeferencing. In contrast, LiDAR campaigns generally incurred higher acquisition costs and took considerable pre-flight planning, with post processing largely involving quality and coverage checks, as well as point classification but this process could still take several months. These pre-flight planning requirements increased the minimum economical area to around 5 km² and favoured combined regional acquisitions.

Overall, aircraft offer an appealing combination of high payload, flexible deployment, and large-scale capabilities. This survey did not consider helicopter operators but these platforms can be adapted to carry similar sensors at lower altitudes and slower speeds, albeit for smaller areas. The key limitation of aircraft was the relatively large minimum area and high fixed costs. For smaller tasks with high repeat or rapid deployment alternatives such as unmanned aerial vehicles (UAVs) may offer an appealing alternative.

Unmanned aerial vehicles

UAVs (sometimes referred to as unmanned aircraft systems (UAS) or Remotely Piloted Aircraft System, RPAS)) have recently attracted significant attention as potential sources of remotely sensed data and as platforms for a range of novel tasks such as security, bird control, chemical/spray applications and many others. These platforms emerged out of a combination of trends including miniaturisation, improvements in battery technology, low-cost digital image sensors, and high-accuracy global navigation systems such as Navstar GPS (US), GLONASS (Russia), and BeiDou (China). Military and recreational applications continue to dominate the market for UAVs, with dedicated remote sensing applications only now emerging as a significant market segment (Pajares, 2015; Watts, Ambrosia, & Hinkley, 2012). Until recently, UAVs for remote sensing required significant systems integration effort by scientists or engineers for particular applications (Jones, Pearlstine, & Percival, 2006). Nonetheless, the availability of remote sensing data from a cheap, accessible, and easily deployed source has spurred strong interest in the use of UAVs for both research and practical operations (Anderson & Gaston, 2013; Toth & Józków, 2016) and this has spurred the rapid advancement of the commercial UAV sector. Fully integrated solutions such as the senseFly eBee (Parrot AR, Lausanne, Switzerland) and DJI Matrice (DJI, Shenzhen, China) have greatly simplified UAV operations, providing an integrated platform with flight planning and sensor control capabilities. Cloud-based image processing tools such as [Pix4D Cloud](#) and [ATLAS MicaSense](#) have simplified extraction of useful imagery products for a range of tasks without the need for specialised computer hardware. Sophisticated open-source alternatives such as [OpenDroneMap](#) also provide high-quality image processing for data collected from UAVs. These factors have made it practical for non-specialists to purchase and operate UAVs and to collect and process imagery for a wide range of tasks. The market for contract UAV data collection has also evolved rapidly in New Zealand. Many existing forestry sector service providers have added UAV services to their portfolio and a range of new entrants serving other industries such as agriculture and mining have sought to enter the forestry market.

To explore the uses and cost efficacy of UAVs for forestry applications, Scion conducted interviews with a range of established and new UAV operators from New Zealand and Australia. These results were augmented with Scion's internal experiences operating and contracting UAV to collect data for research purposes. Our results include standard UAV data products such as RGB and multispectral imagery as well as emerging products such as high-density LiDAR from UAVs. The early status of some companies and services meant that prices and products varied greatly between providers, as did the level of processing and services. For example, some operators delivered only raw imagery sets while others preferred to deliver only the final products to a contracted specification. In the Australian market, derived data products such as the provision of maps showing stem density of coppiced stands estimated from imagery were available from some service providers.

Costs

Indicative costs for UAV imagery are shown in Table 3. Costs were highly variable and contingent on many factors and should be seen as indicative figures only. A key point of difference from aerial and satellite imagery was the lack of a minimum area for UAV data collection, with smaller jobs often priced at an hourly or daily rate. Larger jobs attracted lower rates for both acquisition and processing; however, the large volumes of data requiring processing increased the turn-around time for final products. It was noted that smaller acquisitions could often be processed in the field on the same laptop used for flight planning and delivered immediately to the client. Several providers had switched to offering a daily rate for data acquisition with craft, CAA certified pilots, data processing, and travel included in the price. Prices for this service ranged from \$2500 - \$3000 per day, with contracts lasting several days attracting a discount. Acquisition costs were strongly impacted by two factors: choice of craft and installation of ground control points.

Table 3: Indicative costs for UAV services in New Zealand.

General contractors	Notes	Cost (NZ\$/ha)	Minimum area	Maximum area
RGB + Multi-spec	Fixed wing, raw data	\$3 - 10	Min 1 hr charge @ NZ\$250-350	100 - 2000 ha / day (craft dependent)
RGB + Multi-spec (RAW) Multirotor Processing	Multi-rotor, raw data	\$5 - 10 Plus \$1 – 5	1 - 2 day turnaround	50 - 100 ha / day (typical multirotor) 1 - 2 week turnaround
Forestry Specific				
RGB + Multi-spec	No ground control	\$10 - 25	None, but few jobs < 30 ha	100 - 2000 ha (craft dependent)
RGB + multi-spec	Ground control	\$50 - 125	30 - 40 ha	60 - 100 ha (2000-4000 ha if RTK/PPK only)
LiDAR	Incl. survey and processing to DTM	\$110		

A single contractor offered UAV LiDAR acquisition; however, forestry was a relatively new addition to the service offering with most of their LiDAR work focused on mining or urban survey. The LiDAR unit offered produced very high density point clouds but limited options for forestry-specific processing (e.g. classification and noise removal) were available. Indeed, many UAV LiDAR sensors currently available are adapted from automotive applications and included multibeam laser scanners that make registration and calibration complex. These sensors may work well on hard, regular surfaces but Scion's experience has shown that multibeam sensors over dense foliage and forested areas have poor rates of penetration and produce an unacceptably high level of noise and misregistration. More sophisticated UAV sensors such as the VUX-1UAV or miniVUX-1UAV (Riegl, Austria) have recently become available. These sensors are well suited to forestry and produce multiple returns per pulse with very high levels of precision; however, costs for these units may exceed NZ\$300,000 depending on the configuration chosen and it is unclear if use of these sensors on a UAV is desirable or holds the same cost advantages as other UAV remote sensing methods.

Choice of Craft

Nearly all commercial UAVs use either multirotor or fixed wing configurations. Table 4 summarises indicative costs for common UAVs and sensors used by many contractors and Scion. Multirotor craft have higher payload capacity, increased stability, no minimum airspeed, and simplified landing and take-off requirements. The carrying capacity of larger multirotors allowed simultaneous acquisition of RGB and multispectral imagery. These craft are also well suited to heavier, emerging UAV sensors such as LiDAR and hyperspectral cameras. Surveyed operators favoured multirotor craft for smaller areas, or for tasks requiring very high resolution imagery (low GSD) with high overlap. The maximum area for multirotor craft depended heavily on payload and campaign settings but several operators suggested 100 - 150 ha per day was the maximum economical area. Fixed wing craft offer much greater flight time at the expense of payload. These craft were favoured for general aerial mapping using RGB or multispectral imagery. Operators experienced with forestry work noted these craft were constrained by the need for a clear

launch and landing area. Newer high-resolution cameras (>20 megapixels) have partially compensated for the inability of fixed-wing craft to fly low and slow, but tasks requiring high overlap still necessitate repeated overflights. The maximum area for fixed-wing craft varied greatly depending on the model, with newer platforms such as the eBee Plus that allow rapid battery changes and easy launching capable of capturing over 4000 ha per day for basic imagery. Multispectral imagery also impacted on the time and cost of data acquisition, often requiring repeated, low-altitude flights due to the low resolution of existing cameras (MicaSense RedEdge resolution: 1.3MP); however, newer multispectral sensors feature much higher resolutions (8.3MP - 4K resolution) that will likely reduce the flying time required and increase the area that can be economically flown using UAVs.

Table 4: Indicative costs for typical UAVs hardware and sensors suitable for forestry.

Make	Model	Price (NZ\$)	Endurance (min)	Payload and capacity
Craft				
Multirotor				
DJI	Phantom Pro 4	3000	25	4K 20MP RGB camera
Aeronavics	BOT	5000	25 - 30	Most RGB or multispectral cameras up to 1.2 kg
Altus	LRX - heavy lift	50,000	25	Interchangeable gimbals for custom payload - up to 4 kg; Stable in high winds; Multi-sensor payload
Fixed Wing				
senseFly	eBee Plus RTK/PPK	62,000	59+	RGB, Multispectral, and thermal infrared
Sensors				
Sony	ILCE A6000	1000	360 shots/battery	25 megapixel RGB
MicaSense	RedEdge	7000	2.7hrs from 11Wh craft	5 band multispectral

Ground Control

Without the installation of ground control points, UAV acquired imagery can be expected to have a positional accuracy of 6 - 12 m. Installation of ground control points (GCPs) by surveying markers or landmarks spread across the scene that appear in the imagery offers a range of benefits. GCPs improve the overall vertical (for 3D GCPs) and horizontal positional accuracy of the orthomosaic, often to sub-meter precision. Use of GCPs also improves orthorectification and alignment when using a digital terrain model or other georectified data and enhances the accuracy of area and distance measurements made from remotely sensed imagery (Aguilar, Saldaña, & Aguilar, 2013; Toutin, 2004). The addition of GCPs is also beneficial for co-registering multiple or repeated products e.g. aerial LiDAR, GIS records, and UAV orthomosaics (Liu, Zhang, Peterson, & Chandra, 2007). The survey of commercial UAV operators revealed that addition of GCPs nearly doubled the cost of some data products (Table 3). This finding was supported by Scion's experience, with the installation of GCPs noted to significantly increase data collection time. This is the result of visible GCP markers needing to be evenly distributed across the capture area – a significant challenge in forested areas. High-grade GPS surveys also need to be carried out at each location, adding 10-30 minutes per GCP. Of the surveyed providers, only 4 had access to high-grade surveying equipment. Post-processing costs

also increased, as GCPs needed to be post-processed using licensed software and manually located and marked in multiple images before generating the orthomosaic. One alternative to GCP installation is the use of real-time or post-processing kinematic (RTK / PPK) whereby craft GPS coordinates are processed to a higher level of accuracy either using real-time transmissions from a surveyed reference tower on-site, or by using GPS timestamps to apply corrections to collected coordinates during post-processing. Only 2 providers had access to RTK or PPK equipment, which still required the use of a high-grade GPS to establish the reference location. The significant cost implications of GCP collection mean that future advances in positioning technology could alter the cost efficacy of UAVs for tasks currently requiring GCP acquisition.

Satellite Based Augmentation Service (SBAS)

SBAS services provide improved positional accuracy to GPS users by relaying corrections calculated from a network of ground stations that constantly monitor global navigation satellite system (GNSS) signal accuracy. Augmentation services can be delivered using terrestrial (TBAS) or satellite based (SBAS) data channels. Satellite services offer the advantage that nearly any capable receiver can get access the augmentation service in real-time. Land Information New Zealand and Geosciences Australia are collaborating on an SBAS serving Australasian users. This system will provide three levels of positional improvement (Table 5), including two novel levels of service providing extremely high-precision positional information. Importantly, these services will be available without the need for terrestrial data signals (e.g. mobile networks) and future UAV systems will likely be able to take advantage of this improved positional information. This may offer the opportunity to collect data with a similar level of positional accuracy to that provided by current ground control survey installations.

Table 5: Positional accuracy of planned SBAS systems for New Zealand.

SBAS Service	Hardware	Positional accuracy
Single frequency service (Legacy L1)	Most existing GPS receivers (WAAS/EGNOS compatible)	Better than 1 m accuracy
Dual frequency multi-constellation service (DFMC SBAS L1/L5)	Most commercial receivers supporting GPS + Galileo L5/E5a service.	< 1 m - unknown but significant improvement over Legacy L1 with lower variation in accuracy.
Precise Point Positioning (PPP) service.	Specialised user-segment hardware e.g. tablet/app or microPC with receiver and software.	5 - 10 cm accuracy

The L1 augmentation service will utilise the existing SBAS receiver capabilities built into most modern GPS units that are already widely employed in Europe, America, and other regions served by SBAS. This means that nearly all modern GNSS receivers (e.g. handheld GPS units, mobile phones, satnav units) will be able to obtain sub-meter accuracy without any modifications. The second generation DFMC service will utilise the roll-out of the Galileo GNSS service and a new dual frequency SBAS standard. This standard will require hardware support, but the international use and adoption of this technology is likely to mean that many upcoming GNSS receivers from major brands will support the DFMC service. While the exact gain in positional accuracy is unknown the DFMC service is expected to greatly reduce ionospheric interference, allowing consistently improved positional accuracy for nearly all users. The third service (PPP) uses two dual-frequency broadcasts from GPS and Galileo to provide centimetre level accuracy. This service is highly experimental and initial user-segment access will require a device that can run the real-time decoding software. The 2-year trial of these services is

set to start in June 2017 with a staggered roll-out of the three services starting with the L1 Legacy signal in late June 2017.

Conclusions

The results of the price survey showed that, at present, LiDAR data can only be economically acquired using aircraft and the cost-structure favours larger acquisitions to make these data economical for the current forestry applications. The first generation of UAV LiDAR sensors did not appear well suited to forestry applications and few providers have targeted this market. The ability of satellites to image large swaths of the globe from orbit was reflected in the pricing of the imagery, with 100 ha available for around \$1.50. However, the most economical sensors had low resolution and required very high minimum area purchases. Aircraft were most economical for capturing high-resolution imagery over large areas but were not well suited to rapid acquisition of small areas. UAVs filled this niche, allowing rapid, repeated acquisition of very high resolution imagery of areas up to ~ 100 ha. The weight constraints limited the range and sophistication of sensors but this space has evolved rapidly and it is reasonable to expect continued improvements in sensors and craft. These improvements, along with new technologies such as SBAS may see the role of UAVs expand to include LiDAR acquisition and to cover larger areas at reduced cost.

Wind Damage Assessment

Background

Severe wind events are a major source of forest disturbance in many global ecosystems (Gardiner et al., 2013; W. Wang, Qu, Hao, Liu, & Stanturf, 2010). Damage caused by high winds from tropical depressions (hurricanes) can cause extensive damage to large areas of forest and these events are often associated with long-term changes in forest ecology (W. Wang et al., 2010), increased risk of fire (Myers & van Lear, 1998) and reduction in carbon storage (Boutet & Weishampel, 2003).

Although New Zealand is located outside of the hurricane zone, severe winds associated with periodic tropical depressions migrating from the equatorial zone are major causes of wind damage to both natural and planted forests (Martin & Ogden, 2006; Moore, Manley, Park, & Scarrott, 2013). The heavy rainfall accompanying these events can worsen the damage to forests by lowering the resistive strength offered by the soil and root plate, with larger trees and trees on certain soil types being most affected (Martin & Ogden, 2006; Moore & Somerville, 1998). For several native species, wind disturbance is often followed by strong recruitment, leading to the creation of even-aged stands that may show greater susceptibility to future wind events. This creates a natural cycle of ecosystem disturbance and recovery on vulnerable sites (Martin & Ogden, 2006; Ogden, 1988). Production forestry in New Zealand is largely confined to extensive forests (1.7 M ha) of exotic *Pinus radiata* D. Don (90%), and Douglas-fir (*Pseudotsuga menziesii* (Mirb.) Franco) (6%) planted across a wide range of sites (FOA, 2016). In these forests, catastrophic wind events can have a strong, negative impact on the financial value of the forest. Moore et al. (2013) define catastrophic wind damage in this forest type as any continuous area of wind damage over 1 ha in size in stands over 5 years of age. The same authors estimate that approximately 63 000 ha of planted forest were damaged by wind between 1945 and 2010. This estimate includes only recorded events and is likely to underestimate the total affected area as a significant portion of New Zealand's forest estate is held in smaller woodlots where records are poorer (MPI, 2016). Historically, the costs of wind damage have largely been through the loss of timber value. More recently, the introduction of New Zealand's greenhouse gas emissions trading scheme has meant that participating forests are liable for loss of carbon stocks due to events such as wind and fire, creating additional risk for forest owners (Moore, Manley, & Park, 2011).

Because of the potential for significant financial impacts, timely information on the scale and severity of wind damaged forest is valuable to forest managers. This information can be used to assess the nature of the damage and to begin planning for harvesting of any recoverable timber. Remotely sensed imagery offers the ability to rapidly survey large areas of forest to assess wind damage. Previously, satellite remote sensing has been used to assess wind damage to forests at regional scales using time-series data from sensors such as MODIS (W. Wang et al., 2010) and Landsat (F. Wang & Xu, 2010). Digital surface models (DSMs) derived from airborne laser scanning and DSMs derived from post-storm aerial photogrammetry have also been used to automatically identify storm damage over large areas of forest (Honkavaara, Litkey, & Nurminen, 2013). Time-series data using other remote sensing technologies such as synthetic aperture radar (SAR) imagery has also been shown to allow accurate but manual identification of wind-thrown forests (Fransson et al., 2007). These methods have largely relied on pixel-based approaches to classifying moderate resolution imagery (Chehata, Orny, Boukir, Guyon, & Wigneron, 2014). Higher spatial resolution imagery provides much more detailed information and can benefit from alternative approaches such as object-based image analysis (OBIA) that leverages the contextual and spectral information available in images (Blaschke, 2010). Application of OBIA to bi-temporal high-resolution (5-10 m) Formosat-2

imagery provided improved classification accuracy (87.8%) of wind damaged areas over a pixel-based approach (Chehata et al., 2014). Many of these approaches have relied on the availability of multitemporal, multispectral imagery that may not be available for affected areas. Furthermore, even high-resolution satellite imagery (1 – 10 m) may not provide the fine-scale information required for emerging methods that provide semi-automated identification and measurement of individual downed stems (Blanchard, Jakubowski, & Kelly, 2011; Szantoi et al., 2012).

In this section, we explore the use of RGB imagery acquired using a UAV as a means of both identifying and mapping wind-thrown forest. A second analysis explored the possibility of using higher resolution RGB imagery to enable semi-automated detection of individual stems using OBIA. UAV imagery can be rapidly acquired after a severe storm and modern fixed-wing craft can cover reasonably large areas in a single flight (~100 ha - see Roles and Cost Efficacy of UAVs). Our analysis focused on the use of high-resolution DSMs and RGB orthomosaics derived from photogrammetry. This imagery does not require specialised sensors and can be readily processed using commercial tools such as Pix4D or open source alternatives such as [OpenDroneMap](#).

Data and methods

An area of forest in the Nelson region affected by a catastrophic wind event in 2016 was identified as the site for this study. Two sets of UAV imagery were collected (Table 6) by Buck Forestry and processed using Agisoft Photoscan. The raw images and craft GPS records were combined and re-processed by Scion using the Pix4Dmapper software application (Parrot AR, Lausanne, Switzerland) to provide an opportunity to contrast the performance of these two widely-used software tools. A range of different software settings were trialled in Pix4D to attempt to improve the quality of the orthomosaic. These settings are too numerous to list but focused on improving the digital surface model (DSM) that largely determines the quality of the final orthomosaic.

Wind-throw assessment (Area 1)

The area chosen for large-scale classification of wind damage covered approximately 120 ha of forest on rolling terrain with approximately 9.3 ha of exposed forest severely damaged by wind (Figure 1). This dataset was used to explore semi-automated identification and mapping of wind-damaged areas of forest using low-cost UAV imagery. Existing harvested areas and pasture visible in the scene were masked from analysis, leaving primarily forested and wind-thrown areas. The focus of this analysis was on the use of accessible tools and methods that are available to forest managers. Classification and post-processing was conducted using a) Mahalanobis distance classifier, b) maximum likelihood, and c) isoMeans unsupervised classification. These methods were selected for their availability in the widely-used ArcGIS software suite (ESRI, Redlands, California). Some analysis was conducted using ENVI 5.4 (Harris Geospatial, Boulder Colorado) but results for the chosen methods are unlikely to vary significantly between packages.

Table 6: Description of key characteristics for datasets collected over wind-thrown forest in the Nelson region.

Data characteristics	Wind-throw mapping (Area 1)	Stem extraction (Area 2)
Imagery extent (ha)	120 ha	14 ha
Ground sample distance (cm/pixel)	7	3
Number of images	681	301
Image channels	RGB	RGB
Ground control	No	No

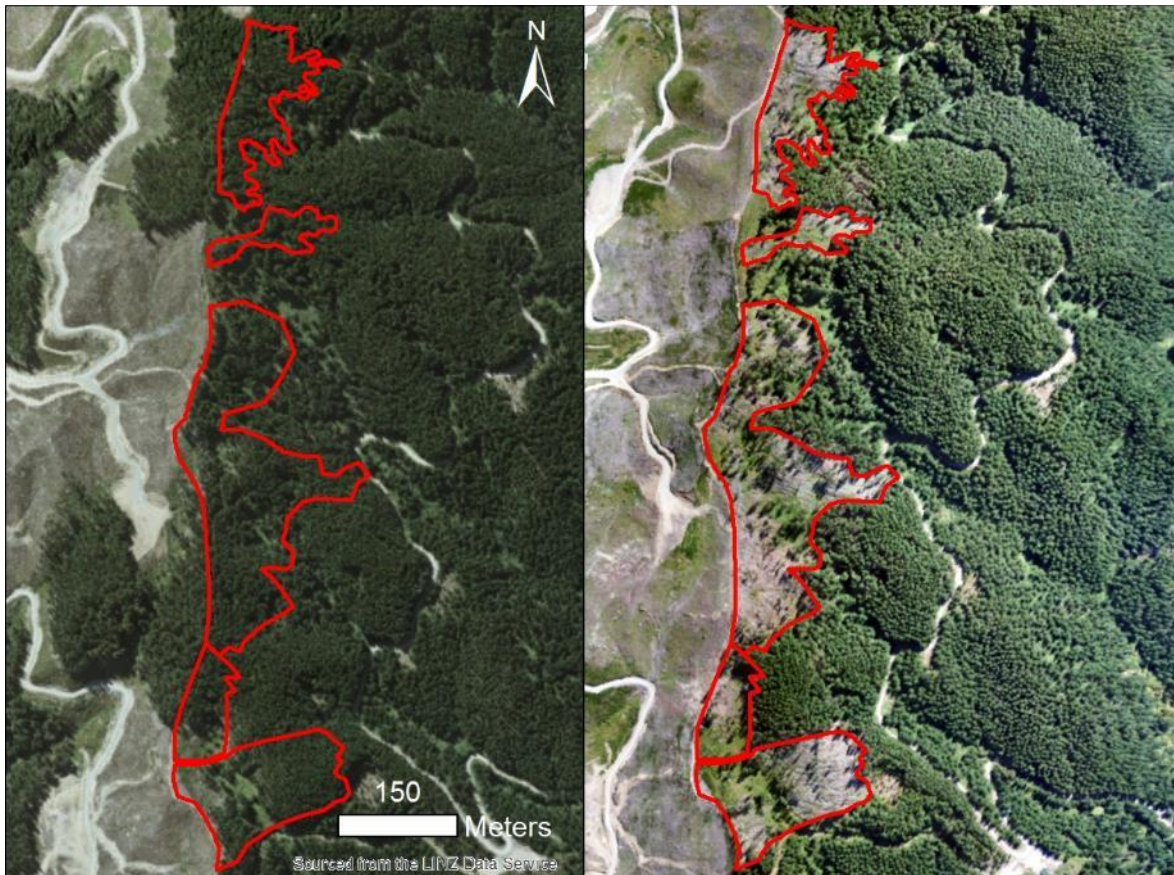


Figure 1: Study site in the Nelson region for large-scale detection of wind damage. The surveyed area covered approximately 120 ha with 9 ha of forest damaged by wind (red areas).

Mahlanobis and maximum likelihood classification are supervised classification methods that require training data to perform classification. A series of training polygons were outlined covering areas representing wind-thrown forest and standing forest. Areas were kept as small as practicable to avoid overtraining and were selected to represent the range of different conditions across the scene. Maximum likelihood classification uses the statistical properties of the pixel values within bands in the identified classes to determine the probability that new pixels belong to a chosen class. Mahlanobis classification is related to maximum likelihood but offers improved speed and assigns pixels to classes using a standardised distance measure that accounts for differences in the variance of the data used to define classes (Abburu & Golla, 2015; Mahalanobis, 1936). The Iso-Cluster classifier is an unsupervised pixel-based classification that attempts to divide the image into the desired number of classes using 'natural' clusters (brakes) in the data across the specified dimensions – in this case, the pixel values across the RGB bands. Mahlanobis and maximum likelihood approaches allowed for probability thresholds to be set, below which pixels are considered 'unclassified'. This option was disabled to force all pixels into a specified class. The optimum settings for the classification were determined by trial and error and will vary by site and scene. Classification results were converted to vector layers and small, irregular polygons were merged to form larger, continuous boundaries for each class. Results were assessed by overlaying the classified areas onto the imagery and comparing the results against boundaries estimated by manually mapping the damaged areas using the imagery and a GIS.

Stem extraction (Area 2)

A second area to the North of Figure 1 was identified to test the feasibility of individual stem identification from UAV imagery. The area covered approximately 14 ha and contained a large area of forest with severe wind damage (Figure 2).

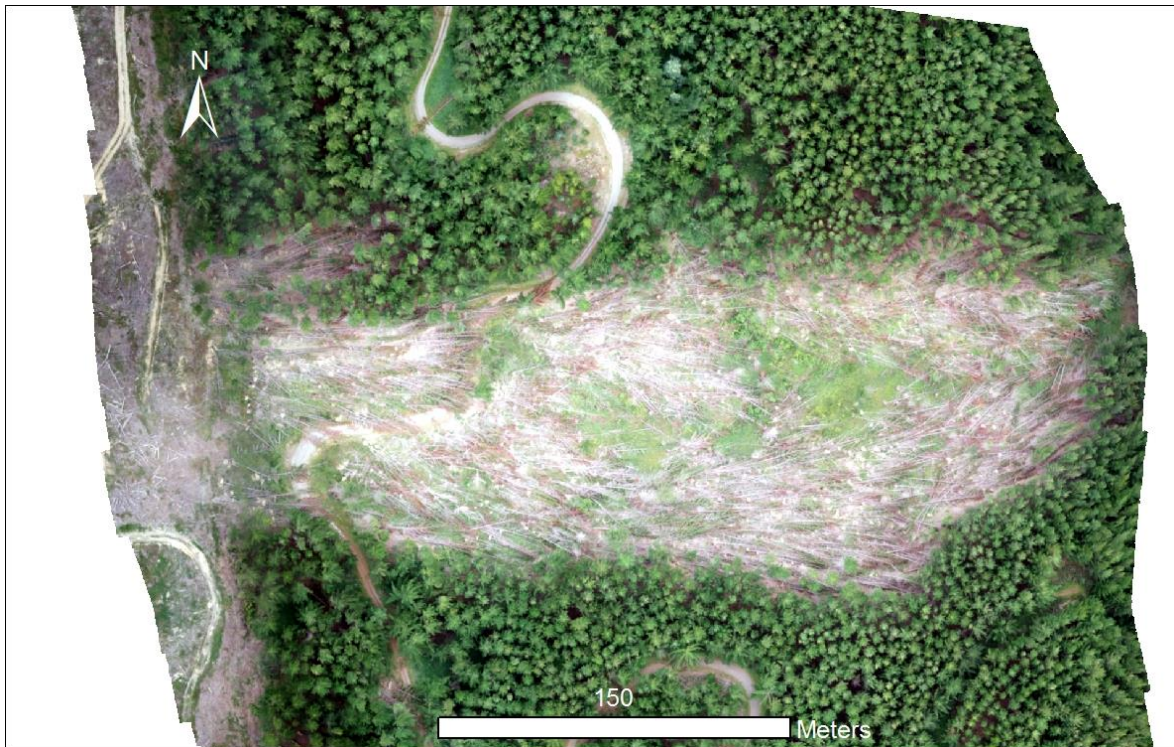


Figure 2: Second area with severe wind damage identified to test identification of individual stems.

A higher-resolution survey was conducted in this area to facilitate the OBIA approach (Table 6). The spectral and contextual properties of the stems were used to define a rule-based classification to separate stems from background vegetation. Results from the rule set were refined using geometric filters and exported as a vector layer. The key criteria for this analysis was the ability to extract straight lines identifying the general outline of stems. The ruleset was developed on a small subset of the image and then later applied to the remainder of the image.

Results

For un-forested areas, both Pix4D and Agisoft Photoscan produced similar quality orthomosaics. Results for Agisoft generally took longer to process but, over forested areas, the faster Pix4D processing generally produced results with a lower level of detail and significant blurring of canopy features (Figure 3), indicating poorer matching of canopy pixels across images. Pix4D offers advanced controls for fine-tuning results over vegetated areas but settings could not be identified using the data available to match the results obtained from Agisoft. Flight settings impacting forward and side image overlap may also have improved Pix4D results. Previous experience with this software at Scion has demonstrated that sacrificing some resolution can often improve the quality of the final orthomosaic. Lower resolution imagery is unlikely to significantly impact large-scale classification tasks such as detection of wind-thrown forest. For this project, the differences in fine-scale detail with higher altitude imagery may not have impacted classification based on spectral properties and analysis using textural metrics may be robust to still greater reductions in resolution but this was not tested.



Figure 3: Comparison of images produced by Pix4D (above) and Agisoft Photoscan (below).

Unsupervised Iso-Cluster classification performed poorly (results not shown) with pixels assignment failing to isolate wind-thrown areas from standing forest. The classification was dominated instead by harvested areas and roads although these areas were poorly defined in the classified imagery. Some settings did allow Iso-Clusters to identify stem pixels but the classification was too crude to be useful. As such, no further unsupervised methods were applied and analysis focused instead on supervised classification methods.

Mahlanobis and maximum likelihood classification methods both performed well and produced nearly identical classification results. The Mahlanobis operation offered faster classification of the image and was chosen for subsequent analysis. This method identified 10.8 ha as compared to 9 ha identified manually from the orthomosaic (Figure 4). The discrepancy of 1.8 ha could be partially attributed to a tendency for the road segments to be classified as wind-thrown forest due to the spectral similarity of stems, exposed ground, and the unsealed road. Canopy gaps filled with green vegetation were also occasionally included as forest. These errors could be resolved by masking road or sparsely forested areas or, if desired, including additional training classes to represent these areas. The small errors in misclassification did not warrant the increased computational time associated with multiclass classification. The Mahlanobis supervised classification also offered some advantages over manual mapping. The pixel-by-pixel classification was able to provide a much more detailed outline of wind-damaged areas than was practical using manual delineation (Figure 4). The process correctly identified standing trees, unaffected areas, and some wind-damaged areas that were missed during manual mapping. Both classification methods had a tendency to produce fragmented, irregular polygons at an impractical level of detail and use of a filter to merge polygons below an area threshold was required to simplify the boundary between standing and damaged forest. The vectorised boundaries were used to compute and report area statistics.



Figure 4: Results from Mahlanobis classification of standing and wind-thrown forest. Approximately 10 ha of damaged forest was identified.

Stem extraction was considerably more complex than the binary classification process used to identify wind-thrown areas of forest. Stems had high reflectance in all bands, but exposed branches with similar properties confused initial classification efforts based only on spectral properties. The blue and green bands showed the greatest contrast between stems and branch pixels due to the mass of senescing needles attached to many of the branches. Assigning each pixel the median value from a 5 x 5 pixel kernel using the blue

band allowed colour differences to be used to 'erode' the branches while stem pixels with many similar adjacent pixels were less affected. Stems overlaying each other also confused rule-sets designed to extract continuous stem lines. A process using both spectral and geometric rules was identified as offering the best results:

- 1) A median filter was applied to the blue band using a 5 x 5 pixel kernel to generate a fourth band with 'eroded' branch features.
- 2) Morphological dilation further reduced the visibility of branches.
- 3) A combination of blue, green and the band produced in 2) were used to produce a contrast segmented image.
- 4) Bright areas were classified as stem candidates.
- 5) Candidate areas were merged and re-segmented according to shape criteria.
- 6) Elongated, spectrally homogenous areas were merged and classified as stems.
- 7) Polylines outlining the stems were exported and overlaid onto the orthomosaic.
- 8) The rule-set was applied to a larger region to identify stems outside of the training area.

The purpose of this ruleset was to explore automated identification and the majority of stems within the scene were at least partially identified by the OBIA method. The ruleset showed moderate success at delineating individual stems (Figure 5). Bare ground and uprooted root plates caused some misclassification due to their spectral similarity to exposed stems. Larger branches made it difficult to choose a single threshold length to isolate only intact stems. This resulted in some fragmented sections of stem, especially where green boughs covered a portion of the stem.



Figure 5: Stem extraction using object-based image analysis based on spectral and geometric properties of image objects. Green lines show the polylines produced by application of the final ruleset.

Discussion and conclusions

The results of this analysis suggest that simple RGB imagery acquired from UAVs can be used to identify and map wind-thrown forest with a level of accuracy similar to manual delineation. Change detection methods have been widely-used to identify forest damage but rely on the existence of suitable time-series data covering the affected region (Honkavaara et al., 2013; F. Wang & Xu, 2010; W. Wang et al., 2010). The demonstrated approach avoids this requirement by using supervised classification only on post-storm imagery. This approach has the added advantage that RGB imagery from UAVs is readily available and very-high resolution imagery can be acquired over large areas at short notice. The classification methods based on Mahalanobis distance are efficient enough to be readily applied to large areas that might take considerable time to manually inspect and digitise using a GIS. Based on our results, classification rulesets also appear likely to provide finer-scale detail than digitisation.

Previous work has often relied on the availability of multi-spectral images to perform classification based on vegetation indices (W. Wang et al., 2010) or use of more sophisticated classification techniques. Use of these data and methods would likely allow misclassified areas in our analysis such as roads and understory to be refined but these methods require more expensive software and sensors that sacrifice some spatial resolution for increased spectral resolution. Overall, the process identified represented a simple and effective means of identifying and mapping wind-thrown areas. The vectorised results obtained were also suitable for transfer into a GIS for tasks such as updating stand records or estimating lost volume.

Identification of individual stems from higher-resolution imagery showed promising results. Similar work has focused on the use of LiDAR data to detect downed stems (Blanchard et al., 2011; Szantoi et al., 2012) but these data can be expensive to acquire, especially if the wind-affected areas of forest are spread across the landscape. Using only morphological and spectral properties on a small area of rubber plantation forest, Duan, Wan, and Deng (2017) identified stems with 75.7% completeness but the method struggled to account for confusion with other objects and assessed only a small area of forest. Application of OBIA to extract stems has the advantage of using the geometric, spectral and contextual properties of stems and has been used with LiDAR data to identify downed stems in standing forests to assess habitat and fire fuel levels (Blanchard et al., 2011). The method presented appeared to provide modest levels of accuracy but lacked a validation dataset to compute completeness and accuracy metrics. Based only on visual inspection, the major errors were errors of commission in regions where stems were obstructed by branches containing green needles. The nature of OBIA means that further refinement of the ruleset could address these challenges by 'growing' stem regions towards other fragmented areas or integrating the DSM data to identify the raised profile of stems. This depth of analysis was outside of the scope of this project, but based on this analysis we concluded that high-resolution RGB imagery acquired from UAVs may be used to identify the majority of larger stems in similar contexts. Imagery may also be more practical than field survey on wind-thrown sites. These areas can be challenging and hazardous to move around in, especially on steep terrain.

In practical terms, most forest managers would primarily be concerned with identification of affected areas to facilitate post-event value recovery operations and to update stand records. For large estates, methods such as low-resolution satellite imagery (e.g. RapidEye, see Table 1) or aerial surveys after a large storm may be more economical as a means of locating affected areas. UAV imagery acquired over identified areas could then complement these methods by providing more detailed views of the scale and severity of the damage. Based on the findings of this work, standard RGB UAV imagery acquired at a moderate resolution appears well suited to aid in planning for value recovery and updating of stand records.

Automated Cutover Detection

Background

Satellite remote sensing is uniquely suited to monitoring forest disturbance at a global level. Since the advent of these technologies, methods have been developed to both quantify forest cover and to monitor changes in forest cover at large-scales (J. C. White, Wulder, Hermosilla, Coops, & Hobart, 2017; Wilson & Sader, 2002). Modern computing methods and an increase in the spatial, spectral, and temporal resolution of remote sensing data have combined to allow quantification of forest change over several decades at a global level (M. C. Hansen et al., 2013; Matthew C. Hansen, Stehman, & Potapov, 2010) and have enhanced knowledge of the total forest cover across a wider-range of biomes (Bastin et al., 2017). Much of this work has focused on identifying forest loss from factors such as illegal logging or land use change in order to address topics such as climate change and biodiversity loss (M. C. Hansen et al., 2013; Keenan et al., 2015). Modern platforms such as Global Forest Watch integrate remote sensing change detection to allow rapid detection and reporting of forest harvest activities at a global scale with results available online for anyone to access (GlobalForestWatch, 2017; Kennedy, Yang, & Cohen, 2010; LandsatFACT, 2017). However, these methods are by necessity coarse and do not always accurately separate out land cover classes or reflect gains in forest cover attributable to increases in plantation forestry as a land use (Tropek et al., 2014).

New Zealand's forests are not subject to many of the same pressures (e.g. wildfire, illegal logging, and shifting agriculture) that have driven the development of these global forest monitoring systems. In New Zealand, application of change detection methods for managed forests is likely to focus instead on forest management and operational applications such as identification of wind-thrown forest, disease outbreaks, and cutover assessment that require a level of spatial and temporal resolution often unavailable from tools targeting large scale degradation or global trends in forest cover. Moreover, the vast majority of New Zealand's change in planted forest cover is the result of (legal) new plantings or harvesting of existing forests. Therefore, many of these large-scale methods and approaches are unlikely to serve New Zealand's forest managers well. Instead, methods for detecting forest cutover would be more useful if they could provide rapid, accurate mapping of cutover areas to better monitor forest operations.

The imagery and positional information available from UAVs has the potential to enable rapid and ongoing mapping of harvest operations under a range of weather conditions and in difficult sites (Grenzdörffer et al., 2008; Horcher & Visser, 2004). These data could provide forest managers with spatially-explicit information on harvest activities to: 1) better manage harvest crews, 2) improve reconciliation information, 3) update stand and GIS records, 4) link geospatial data to harvester data, and 5) improve logistical planning. Use of UAVs has not been widely explored for these applications (Tang & Shao, 2015) with most research applications of UAVs focused on forest inventory and pre-harvest survey (Puliti, Ørka, Gobakken, & Næsset, 2015; Tang & Shao, 2015; Wallace et al., 2014).

Studies using satellite imagery have shown that harvested areas can be detected with a high-level of accuracy (87.5%) using moderate resolution imagery (Steven A. Sader & Legaard, 2008). This is not surprising given the strong spectral differences between harvested areas and standing forest that can be used by various classification methods. Infrared reflectance and vegetation indices utilising this portion of the spectrum such as the normalised difference vegetation index (NDVI) and the normalised difference moisture index (NDMI) appear to be particularly well suited for classification (S.A. Sader, Bertrand, & Wilson, 2003; Steven A. Sader & Legaard, 2008). These bands are not available in low-

cost RGB imagery acquired from UAVs, limiting the applicability of these methods. However, modern machine learning techniques can often achieve excellent classification using different types of remotely sensed data including basic RGB imagery (C. Huang, Davis, & Townshend, 2002; Mountrakis, Im, & Ogole, 2011; Pal & Mather, 2005).

This section describes an experimental UAV platform designed to facilitate rapid, autonomous identification and mapping of harvest boundaries using only RGB video and imagery from a low-cost camera mounted on the UAV. The experimental platform was designed to automatically process imagery in real-time to identify and follow the boundary between forest and harvested areas. The design, integration and testing of this system was supported by Scion Research and the University of Canterbury and carried out as part of a Masters in Engineering thesis (Hunt, 2016). The following sections and figures are abbreviated and adapted from the final thesis and project reports provided to Scion.

Methods

Training data

A specialised UAV was designed and built to test the feasibility of autonomous cutover tracking and mapping. The system was based around a Steadidrone QU4D (Steadidrone, Knysna, South Africa) multirotor craft with a maximum payload of 800 g. A light-weight laser rangefinder was integrated to provide altitude detection and control. The UAV vision system was based around a light-weight consumer grade webcam mounted on a two-axis gimbal. Video from the camera was transmitted wirelessly to a ground receiver to allow real-time monitoring of the UAV. The video was also fed into a single-board computer (Minnowboard Max and Turbot, Intel Corporation, California, USA) to allow real-time processing of imagery to detect and track the forest cutover boundary. Guidance and flight control for the UAV were provided by a programmable flight controller connected to the single-board computer. This allowed the guidance system to be controlled using the results of the image processing algorithm running on the on-board computer.

The guidance and vision systems were developed using a software simulation of the flight controller that could simulate navigation and craft control based on simulated or actual inputs from the different sensors. The vision-based navigation system was developed and tested using a series of training datasets (Figure 6) showing various forest cutover scenes in images and video collected from aerial survey and using Scion's UAV. The imagery was collected at a range of altitudes using RGB, infrared, and multi-spectral sensors. Ground-truth GPS survey of the actual cutover line was also carried out at one test location to allow comparison of the guidance systems edge path against the true edge.

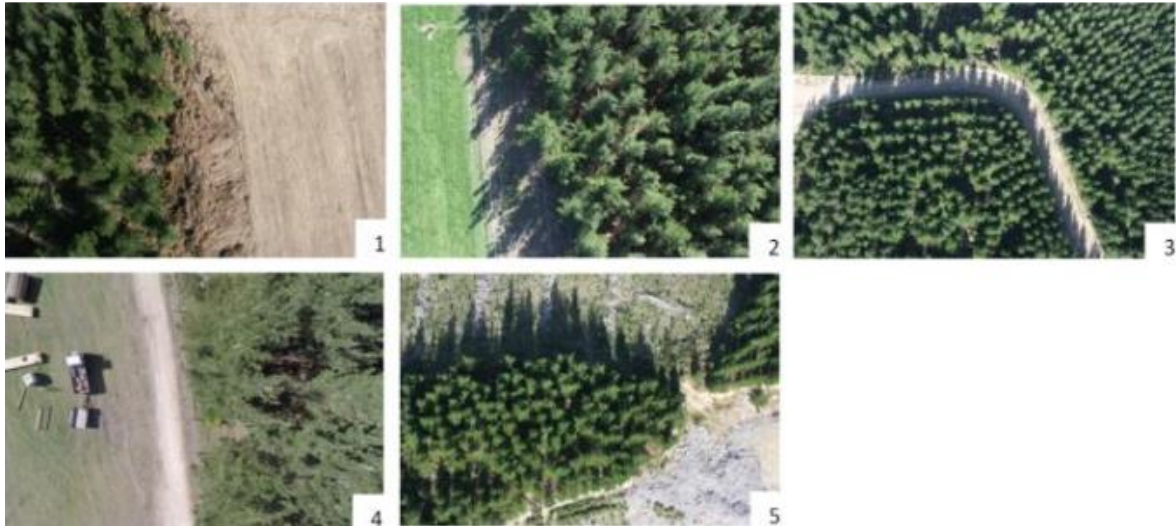


Figure 6: Examples of different scenes used to develop the cutover detection and tracking algorithm.

Algorithm development

The primary objective of the project was to develop an algorithm that could locate the cutover edge with a level of accuracy and reliability that would allow the demonstration craft to be guided by the location information in real-time. The majority of the project was concerned with development of this algorithm. Other objectives focused on expanding and augmenting the edge-tracking system to address high-level navigation decisions such as maintaining altitude and position over the cutover boundary and altering air speed and direction in response to different events such as loss of the cutover edge.

A range of algorithms were explored to allow the vision system to detect and track the boundary line between cutover and forest. Although multispectral imagery has previously been identified as useful for identifying harvested areas (S.A. Sader et al., 2003; Steven A. Sader & Legaard, 2008) this imagery required specialised sensors and output formats. Techniques that allow 3D scene awareness such as structure from motion (Ullman, 1979) and optical flow methods (Hérissé, Hamel, Mahony, & Russotto, 2010; Hérissé, Russotto, Hamel, & Mahony, 2008) were also examined but these were observed to require significant computational power or were negatively affected by the lens distortion present in cheaper RGB sensors used to capture the training images and video.

Because of these limitations, a range of image processing techniques suitable for use with standard RGB imagery were identified for development of the final algorithm. Three methods were highlighted for detailed investigation:

- 1) Simple binary thresholding of images produced using a colour space transformation method that maximised contrast between the forest and cutover. Threshold values in the transformed space were determined by trial and error and used to produce a binary image (forest / cutover). The binary classification was then filtered and refined before application of a contour detection algorithm to find the cutover edge.
- 2) A support vector machine (SVM) learning algorithm was trained using transformed example images of forest, cutover, and mixed areas covering a range of different conditions. A total of 6 derived image features were used in both linear and radial kernel SVM classifications. The SVM was used to classify images and a contour discovery algorithm was applied to the classified image to extract a line

representing the cutover edge. A refined version of this method was used for the supplementary testing conducted using a second iteration of the UAV system.

- 3) A method combining the classification results from both the colour-transformed method (1) and the SVM approach (2) was developed. Results were combined to utilise the different advantages of each method. A boundary detection method was applied to the classified image before being combined with a smoothing algorithm to produce a more regular flight-path following the cutover edge. This method was used for flight testing with the first iteration of the UAV system.

These methods were applied to a set of 5 manually classified images to calculate accuracy statistics. The test images were chosen to include different brightness levels, shadow direction, cutover edge clarity, and height above ground (Figure 7). The best algorithm was then applied to a video feed connected to a full simulation of the UAV system to evaluate how the automatic navigation system would control the UAV in response to the cutover edge detected in the test videos. The simulated UAV flight line was compared to the ground-truth GPS track of the actual forest edge. The final algorithm was integrated into the flight control computer along with relevant fail-safe instructions in preparation for use in a series of test-flights.

Flight testing

Incremental testing of the UAV system with increasing levels of complexity was performed to ensure individual aspects were working as expected before proceeding. The tests were set up as follows:

Flight Test 1: The first flight test involved taking the quadcopter for a flight with all supplementary hardware removed to test that the craft, flight controller, and transmitting equipment were behaving as expected.

Flight Test 2: The second flight test added the Minnowboard computer into the navigation loop sending instructions to the flight controller to fly along a simple square with sides of 10 m. This served as a test for the navigation system and of the communication between the flight control system and the Minnowboard computer that would ultimately send more complex navigation commands to follow the detected edge.

Flight Test 3: In the third flight test, the camera gimbal, camera, and video transmitter were mounted in order to test the quality and range of the video downlink as well as the functionality of the gimbal.

Flight Test 4: The fourth flight test involved the testing of the integrated UAV system including the full cutover detection and tracking system. This test was performed at Bottle Lake Forest Park. Technical issues relating to the video downlink and Pixhawk firmware meant that a successful test was not performed. Despite this, performance of the proposed cutover edge algorithm was verified, with the cutover edge being reliably and accurately detected using the combined SVM and colour transformation methods.

Following a crash of the Steadidrone-based system, a second test UAV was commissioned with support from Scion. The software was ported for operation with an Aeronavics Navi UAV and the on-board processing was upgraded to a more powerful system (Intel NUC, Intel Corporation, California, USA). The edge-detection algorithm was adapted to run on the new system and simplified to use only the SVM classifier. A series of test flights were carried out at Bottle Lake Forest using the Aeronavics platform. The edge-detection algorithm was tested in both manual and automatic mode.

Results

UAV System

All sensors, the flight controller, and the single-board computer were successfully integrated and tested. Hardware-in-the-loop simulation (allowing simulation of craft behaviour based on inputs from the sensors and Minnowboard computer) was used extensively to test the modules and to develop the edge-tracking algorithm. This approach greatly simplified the development process and allowed software routines to be thoroughly tested before upload to the actual craft. Overall, the system performed well and identified issues relating to control and motion of the craft were resolved. Flight testing of the UAV system was carried out at a recent harvest site in Bottle Lake Forest park with the permission of Rayonier | Matariki Forests (Figures 7 and 8).



Figure 7: A panorama generated of the site used to test the cutover edge detection and tracking system on-board a UAV.



Figure 8: An image take of the Steadidrone UAV during flight testing at Bottle Lake Forest Park.

Cutover detection algorithm

The results of the two classification algorithms tested individually against the manually classified set of images are shown in Table 7. In simple images (Figure 6, 1 & 2), the colour-transformation classifier narrowly outperformed the SVM classifier. However, the colour-transformation method only outperformed the SVM method by a large amount in one of the tested images and had a mean accuracy rate that was 7% lower than the SVM classifier. The SVM classifiers had poor performance on image four (Figure 6, 4) which was likely due to the distortion of the trees due to the low altitude of the image and the low contrast. Images one and two (Figure 6, 1 & 2) were more typical of the scale used in the training data set. Classification accuracy from image three (Figure 6, 3) using the colour-transformation method was particularly low due to the two regions of forest in the image. Due to the contour selection step of the colour classification, the entire forest section

below the road was ignored. This highlighted the need for a classifier that did not rely solely on colour values and motivated the selection of a combined approach.

Table 7: Accuracy of SVM and colour based forest classifiers applied to five ground truth images.

Image Number	SVM Accuracy	Colour Accuracy
1	96.2%	97.1%
2	94.6%	96.9%
3	92.8%	55.0%
4	81.9%	90.2%
5	85.3%	76.7%
Mean	90.2 %	83.2 %

The flight paths produced by the edge-detection algorithm applied to a sequence of images following the edge of a cutover are shown in Figure 9. The flight path agreed well with the ground-truth forest edge. The absolute deviation of the flight path from the actual edge was 26.2 pixels. Based on the size of tree crowns and tree trunks in the image, there were approximately 11 pixels per metre in this scene, implying an approximate average error of 2.4 m. This discrepancy was largely attributable to the smoothing routine included in the edge detection algorithm that was essential to avoid rapid, irregular adjustments of the UAV during flight.

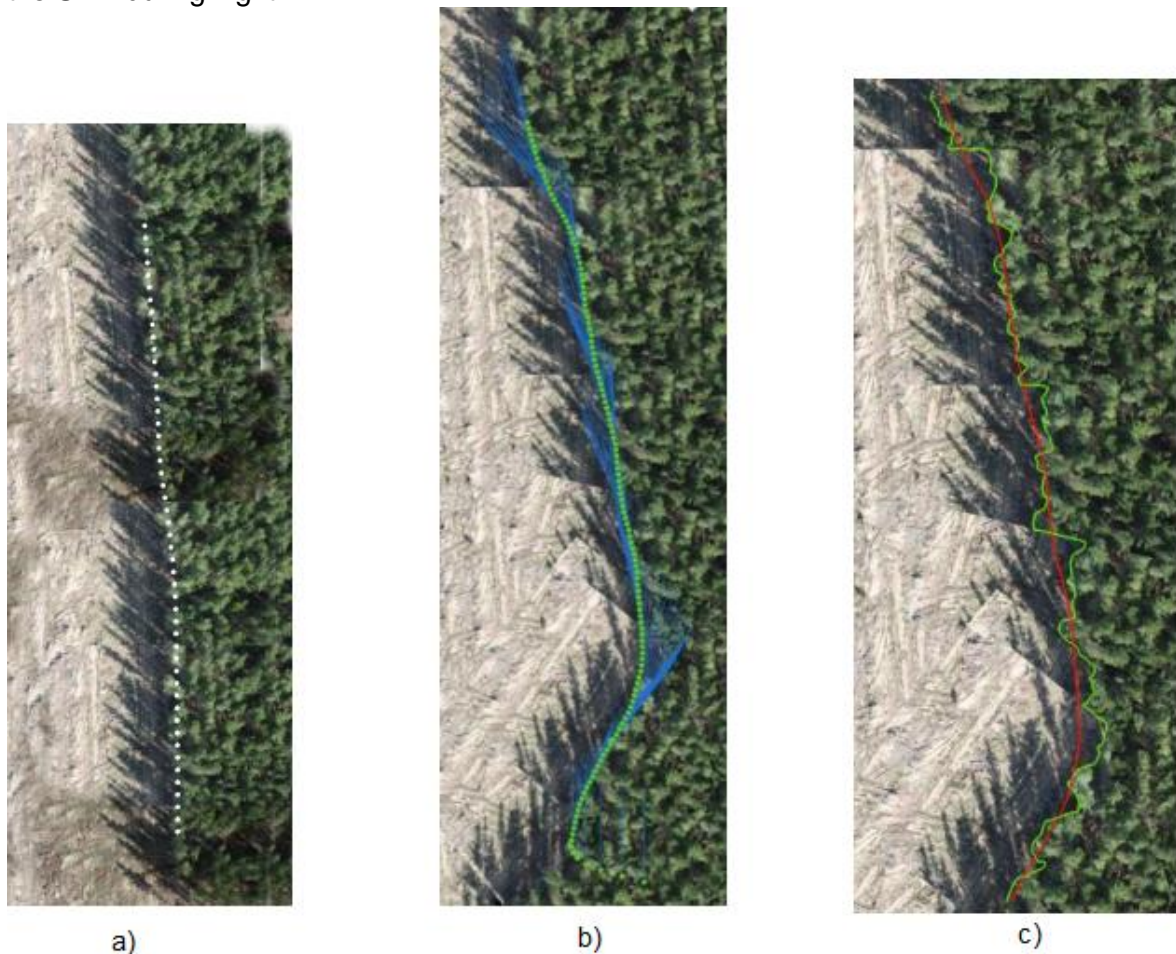


Figure 9: Software simulation of UAV flight path based on cutover edge detection algorithms. (a) Shows the simulated flight path from an early iteration of the algorithm over simple edge features. (b) Shows a later example of the UAV flight path (green) and heading (blue lines) over a more complex edge. (c) Shows the smoothed flight path (red) against the edge as assessed from ground-truth mapping (green).

The algorithm was successfully adapted to run on the Aeronavics UAV and several test flights were carried out using the new platform. Results showed that the improved SVM classifier was more reliable during actual flights. Manual flights showed the software to be accurately tracking the cutover edge and the system was successfully switched into automatic mode. The UAV successfully identified and followed the edge in autonomous mode during this flight.

Discussion and conclusions

These results demonstrated that simple RGB imagery acquired from a UAV can be used to accurately classify forest and cutover areas. The classification results were good enough to enable autonomous navigation of a UAV system programmed to detect, track, and map the cutover edge. The accuracy of the classification results (SVM = 90.2% accurate) compared well to similar research using imagery with higher spectral resolution, where SVM classification was reported as being 87.9% accurate (Pal & Mather, 2005). The Aeronavics based platform further demonstrated that the SVM method alone was sufficient for the task; however, a more powerful CPU was required to perform classification in real-time. SVMs have been widely used in remote sensing and are well suited to the complex image classification and different sensor types encountered in the field. These methods are also transferable to a wide range of image sources and can be used on orthomosaics generated in post-processing rather than real-time video frame as done in this project (C. Huang et al., 2002; Mountrakis et al., 2011; Pal & Mather, 2005).

Previous research has addressed similar tasks such as autonomous tracking of a river centre using a fixed-wing UAV (Rathinam et al., 2007). The simulated mean accuracy of 2.4 m from the SVM method in this test compares favourably to the mean value of 7 m observed in Rathinam et al. (2007) during flight testing. In a forestry context, errors of this magnitude are likely to be lower than those produced used traditional aerial or satellite-based cutover mapping (Figure 10) and could be used to update GIS records and monitor harvest operations with high frequency.



Figure 10: Example image showing manual cutover edge identification from aerial imagery.

The project successfully demonstrated a proof of concept for an autonomous UAV system that can detect and follow the forest cutover edge. Development of the system was complex and suffered from numerous technical challenges. However, use of a commercial grade UAV and upgraded computational systems resolved most of these challenges. A range of commercial UAVs such as the PaparazziUAV (Parrot AR, Lausanne, Switzerland) now offer some form of programmable guidance system. These systems

could potentially be used to further develop and implement methods similar to the demonstrated cutover detection algorithm on top of mature hardware platforms with much greater simplicity.

Future work could also explore further use of a laser range finder to supplement the tracking algorithm and enhance the control functions of the system. For safety reasons, the UAV was only operated in autonomous mode for brief periods. With further development the system could be expanded to include more sophisticated control features for faster flying and to perform advanced tasks such as entering search mode for the cutover at the start of the flight, or after the line is lost.

Post-planting assessment

Background

Within plantation forestry, there is considerable interest in the use of imagery to assess post-planting stocking for quality assessments and to detect mortality of seedlings so that replacement planting can be scheduled in a timely manner. The objective is to achieve a uniform target stand density across new or replanted areas to achieve silvicultural objectives. Mortality of seedlings may be caused by a range of factors such as moisture stress (Villar-Salvador et al., 2012), pathogens (Reglinski & Dick, 2005), herbivory (Bulinski & McArthur, 1999), weed competition, and frost damage (Mason, South, & Weizhong, 1996). Current assessment relies on inspection of a small number of sample plots or transects to assess mortality and identify irregular planting density. This process is laborious and often only a small sample of the total planted area can be economically assessed. UAV-based assessment may offer a means of rapidly assessing seedling mortality and density across large areas. However, most research to-date has focused on mortality of larger trees and little work has examined the use of UAV imagery.

Remote sensing has been widely used to characterise the spatial extent of tree mortality caused by drought stress (Allen et al., 2010; Macomber & Woodcock, 1994; Williams et al., 2010), bark beetle infestation (Edburg et al., 2012; Wulder, Dymond, White, Leckie, & Carroll, 2006), and to study the potential impacts of mortality on regional carbon budgets (C. Y. Huang & Anderegg, 2012). Most research has used satellite imagery to quantify the spatial extent of tree mortality at regional and landscape scales using imagery of a moderate (5 - 30 m) resolution (Fraser & Latifovic, 2005; Meigs, Kennedy, & Cohen, 2011). Over the last decade a growing number of studies have used high resolution (<5 m) satellite imagery to examine tree mortality at finer spatial scales in order to detect mortality of individual trees, or clusters of trees, within a stand (Coops, Johnson, Wulder, & White, 2006; Dennison, Brunelle, & Carter, 2010; Guo, Kelly, Gong, & Liu, 2007; Hicke & Logan, 2009; Stone, Penman, & Turner, 2012). Generally, the use of satellite imagery with a finer spatial resolution has been shown to more accurately classify mortality. For example, recent studies, that investigate mortality from outbreaks of mountain pine beetle (*Dendroctonus ponderosae*), showed classification accuracies ranging from 67- 78% for medium resolution (Franklin, Wulder, Skakun, & Carroll, 2003; Skakun, Wulder, & Franklin, 2003; Wulder et al., 2006) to accuracies of 71-93% when high-resolution satellite imagery was used (Coops et al., 2006; Hicke & Logan, 2009; Joanne C White, Wulder, Brooks, Reich, & Wheate, 2005; Wulder, White, Coops, & Butson, 2008).

Although the utility of satellite imagery has been widely explored, far less research has utilised aerially-acquired imagery at a very fine resolution to characterise mortality. Four-band aerial imagery with a spatial resolution of 30 cm was acquired over lodgepole pine-dominated stands recently attacked by mountain pine beetle (Meddens, Hicke, & Vierling, 2011). The imagery was resampled to 1.2, 2.4, and 4.2 m resolutions and indices derived from this imagery were used to detect mortality using a maximum likelihood classifier.

Imagery with a 2.4 m resolution, which approximated the crown area, provided the highest classification accuracy of 90%. Stone et al. (2012) used multispectral aerial imagery at a spatial resolution of 20 cm to successfully detect drought-induced mortality in *Pinus radiata* D. Don within stands ranging in age from 0-35 years.

The indices used to detect mortality show considerable consistency between studies. Conifer foliage may be damaged and become red due to a variety of agents, such as insects, root rot, fungi, and drought (Vollenweider & Günthardt-Goerg, 2005). Independent of the damaging agent, foliar moisture declines, chlorophyll and other pigment molecules break down, followed by a breakdown of intracellular and cellular structures (Sims & Gamon, 2002; Vollenweider & Günthardt-Goerg, 2005). This change manifests as an increase in the spectral reflectance of red wavelengths and a drop in green reflectance (Ahern, 1988; Curran, Dungan, & Gholz, 1990; Herrmann, Rock, Ammer, & Paley, 1988; Leckie, Teillet, Fedosejevs, & Ostaff, 1988; Rock, Hoshizaki, & Miller, 1988). Consequently, the ratio of red reflectance to green reflectance, which is known as the Red-Green Index (RGI), was found by Coops et al. (2006) to be most effective at separating green tree crowns from red tree crowns in areas attacked by mountain pine beetle. The RGI index and temporal changes in this index were subsequently used to detect attacked crowns in many studies using both satellite imagery (Gartner, Veblen, Leyk, & Wessman, 2015; J. White, Coops, Hilker, Wulder, & Carroll, 2007; Wulder et al., 2008) and four band aerial imagery (Dennison et al., 2010). A similar classifier based on the red and green reflectance bands was used to detect drought-induced mortality from aerially-acquired multispectral imagery (Stone et al., 2012).

Nearly all of this work has focused on detecting mortality on larger trees using imagery from aircraft or satellites. We are unaware of any research that has investigated the feasibility of detecting density and mortality in young plantations with small seedlings. The successful detection and mapping of seedlings will require the matching of the platform, sensor and image analysis method to the information requirements. Previous research shows that detection rates of mortality are high when spatial resolution of the imagery approximates crown area and imagery that includes the green, red bands is collected. This suggests that a UAV, which can supply RGB and multispectral imagery at 3-10 cm resolutions, is likely to provide the most appropriate platform for detection of dead seedlings.

Methods

The trial was carried out at Rangipo in the Central North Island. The site was formerly under fertile pasture and was converted to forestry as part of a Scion led trial. The site included a range of treatments, planting densities, and included site preparation (continuous ripping) in two blocks. This provided a range of conditions for testing the image analysis methods. Table 8 summarises the key characteristics of the data collected.

Table 8: Summary of site flown to test assessment of seedling mortality and density.

Site	Captured (Age)	RGB	Multispec	Notes
Rangipo 1 (8 ha)	April 2017 (8 months)	Yes - 1 cm/pixel	No	Trial site converted from pasture with +- 4ha ripped (East block)

The eastern half of the trial was subject to site preparation (continuous ripping) before establishment. The trial was planted between 22-24 August 2016 and the first RGB imagery was collected in February 2017 with a second dataset collected in April 2017 with higher resolution RGB. The April dataset was used for all analysis due to the higher resolution available; however, weed growth had increased significantly since the

acquisition of the February dataset. The RGB imagery was processed in Pix4D Mapper with the ground control points installed before generation of the orthomosaic.

Multiple attempts were made to capture multispectral data at the location; however, several factors significantly hampered these efforts. The low resolution of the RedEdge multispectral camera (1.3 MP) meant extremely low altitude flight plans were required to obtain adequate resolution imagery of the small seedlings. This necessitated a series of very slow flights and changes in sky conditions such as clouds moving over the sun repeatedly spoiled the data. The changes in reflectance created significant artefacts in the imagery, especially across key bands such as the red edge. This imagery was ultimately excluded from analysis and the approach focused instead on exploring methods to identify seedlings from very high resolution RGB imagery alone. Capturing RGB imagery of the seedlings was greatly simplified by the much higher resolution of typical RGB cameras. Cameras that have a resolution of 20 megapixels or higher are affordable and can be purchased to suit a wide range of UAVs. This greatly increased the practicality of conducting the post-planting assessment. The current generation of multispectral sensors are more expensive and have a considerably lower resolution (1.3 MP MicaSense RedEdge cf. 20 MP RGB Sony). This significantly increases the time and cost of acquiring high-resolution data and may make this impractical for operational use. However, newer generations of these sensors with much higher resolutions (4K) are currently being tested for release in 2017/ 2018. These sensors are likely to overcome many of the challenges noted in this study.

The imagery covered a large area and a manual field survey to identify dead or senescing seedlings was carried out along several transects within the bounds of the trial. Different subset areas of the main trial were identified to develop and test the two approaches trialled. The OBIA analysis was developed using a 0.2 ha subset. The area was clipped out from the main orthomosaic and the position of each seedling (dead or alive) was manually digitised from the orthomosaic. A total of 257 seedlings were identified. This step was accomplished using ENVI 5.4 (Harris, Boulder, CO, USA). The subset area and marked seedlings are shown in Figure 11. The area chosen included a mix of seedlings surrounded by bare earth as well as some areas with significant weed growth. The weeds had similar spectral properties and some had attained a similar height to the pine seedlings. Analysis of training samples showed little spectral separability of weeds from seedlings in the RGB bands, suggesting that supervised classification was unlikely to be successful. The RGR index has previously been used for similar tasks (Gartner et al., 2015; J. White et al., 2007; Wulder et al., 2008) and a new layer (RGR) was computed as Red Digital Number / Green Digital Number for the subset area. The first approach focused on using OBIA to identify seedlings by combining the available spectral and contextual information (Blaschke, 2010). In this case, pine seedlings were taller than most surrounding weeds – casting significant shadows, planted in a regular pattern, and were slightly darker than weeds in the red and green bands and showed increased contrast in the RGR layer. The analysis attempted to develop a rule set encapsulating these characteristics in order to separate out live seedlings from other image features.

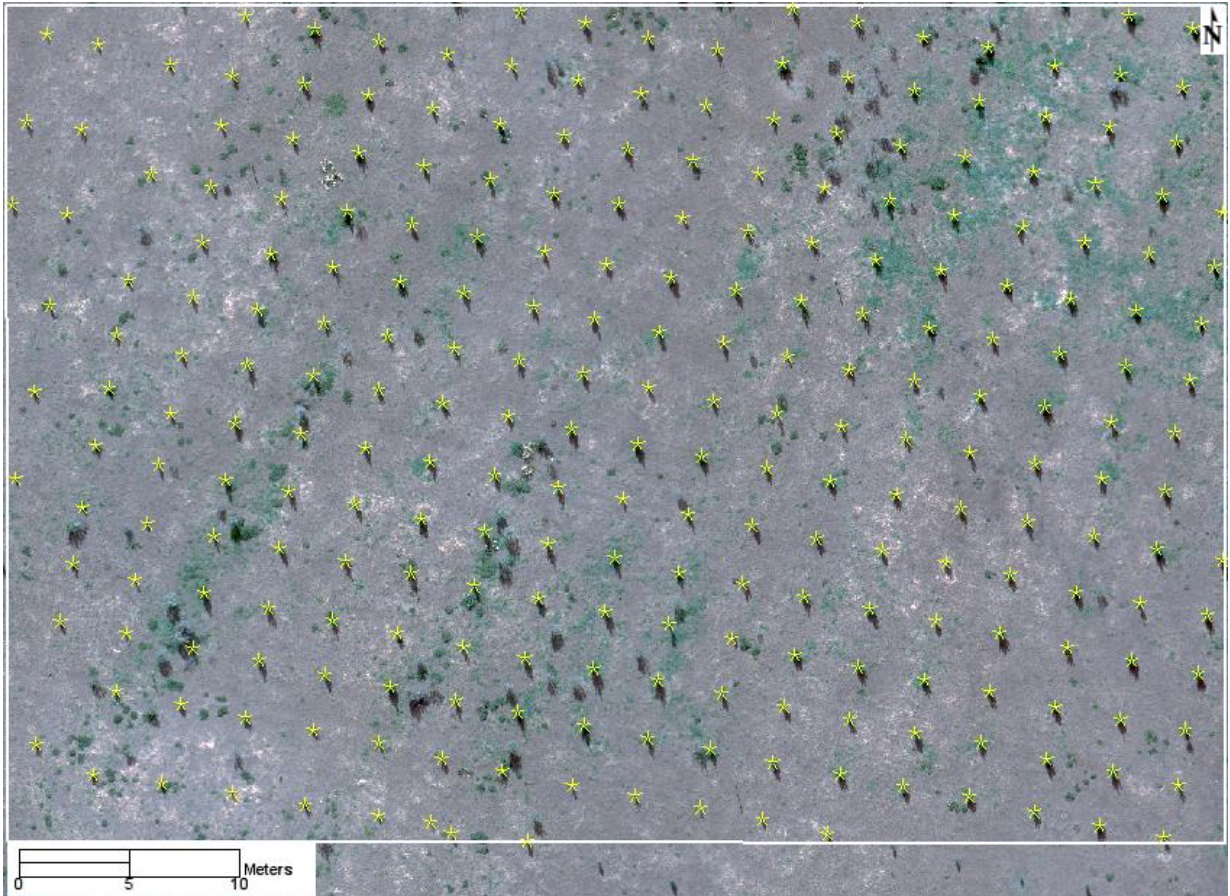


Figure 11: Rangipo RGB data showing a subset of the compartment containing manually identified seedlings (yellow asterisks) used to test an object-based classification.

The second approach used a method based on cross-correlation template matching. This is a well-established image processing and machine vision technique that identifies areas in an image that match a template defining features of interest (seedlings in this case). The template is systematically compared to the target image pixels within a moving window of the same dimensions as the template. The normalised correlation coefficient between the template and the current window is computed and recorded in a secondary image (Briechele & Hanebeck, 2001; Sarvaiya, Patnaik, & Bombaywala, 2009). A correlation threshold can be specified based on the desired level of specificity and sensitivity to identify the best matching areas within the target image. A combination of software tools was used to develop this approach but the commercial package MATLAB (MathWorks, Natick, MA, USA) and the open source alternative SciLab (Scilab, 2012) are capable of sophisticated template creation and matching for image recognition.

The image template was developed using training data from a new 0.8 ha area containing a large number of seedlings (Figure 12). The training process used 400 reference images containing a single seedling each. These data were used to assess the accuracy of different templates derived using each of the bands (RGB) and using different window sizes (15-60 pixels or cm). The best template was then applied to two new regions to assess the accuracy. Each identified seedling was manually assessed and the Type I error (false positive) was computed. A second inspection identified missed seedlings to compute the Type II error (false negative). The second region was located in an area heavily infested with weeds to assess how the template matching algorithm would perform in these areas. An example of this area can be seen in Figure 13.



Figure 12: Training area within Rangipo RGB imagery used to develop cross-correlation template image.

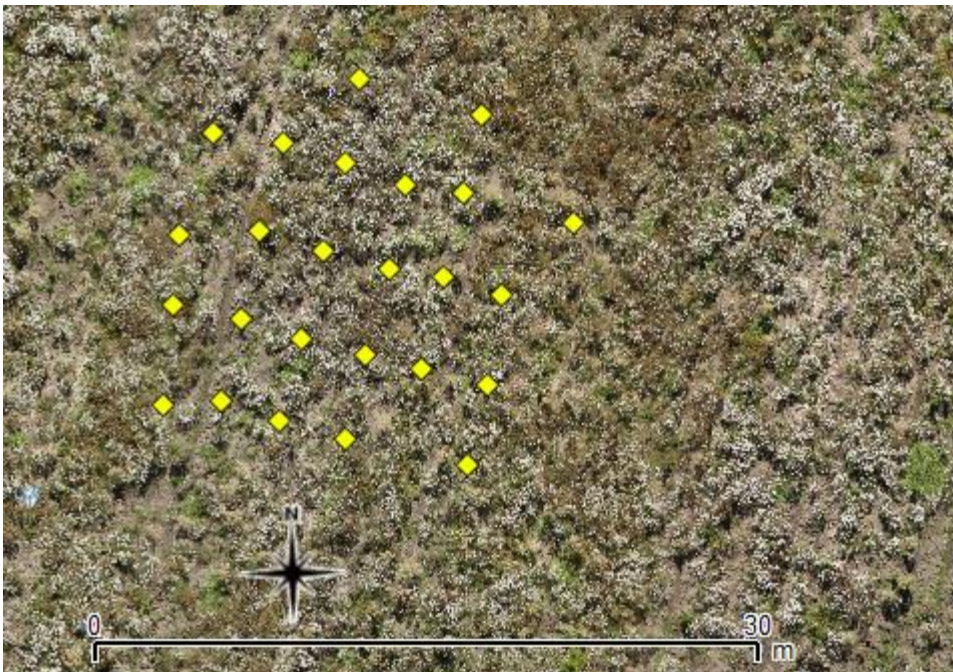


Figure 13: Second test area in heavily weed infested location. Yellow diamonds show manually identified seedlings.

Results

A range of OBIA rulesets were trialled and tested in the first region. The best results were obtained by:

- 1) Separating image components using only the red and green channels. RGR index was not useful and was discarded.
- 2) Thresholding regions with low RGB digital numbers to isolate the shadowed side of the seedlings.
- 3) Thresholding regions with higher green values but low blue values to separate out most live vegetation, and especially the brighter green conifers.
- 4) Classifying shapes that had both bright green pixels in a circular shape that were adjacent to regions classified as 'shadow' as 'candidate seedlings'.
- 5) Filtering out smaller shapes to leave only the remaining objects classified as 'seedlings'.

The centroid of each seedling shape was extracted and compared to the actual locations of seedlings. The results of the OBIA analysis are shown in Figure 14.

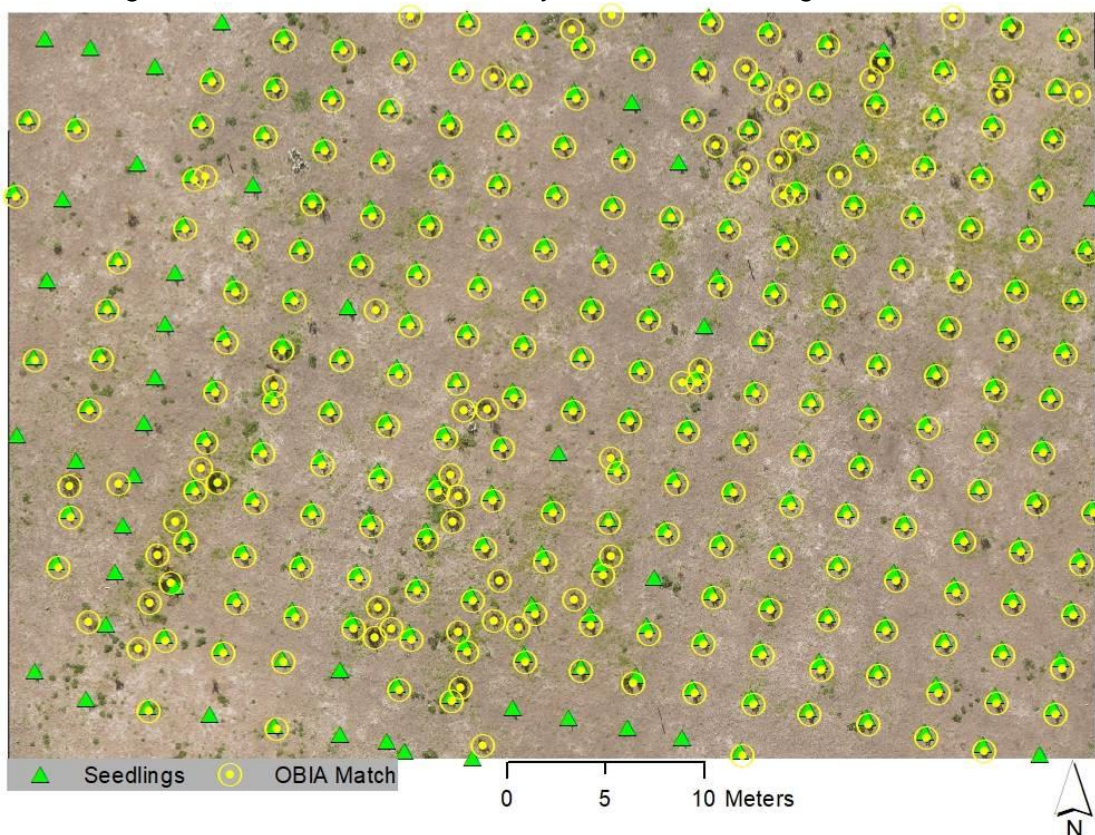


Figure 14: Results from an object-based classification to detect seedlings in RGB imagery.

The centroids for correctly located seedlings were always located on the South East edge of the seedlings, reflecting the influence of the shadow on the shape of the classified objects. The lack of spectral resolution to separate out conifers from weeds was reflected in the rate of false positives. Out of a total of 267 detected seedlings, 46 were false positives. All of these were located on tall, dark green weeds that were confused for seedlings. Dead seedlings were not included in the false positives. The number of false negatives was 36. Most of these were seedlings much smaller than the average size or regions where tall weeds near grass confused the OBIA ruleset. The precision of the classifier (true positives / true positives + false positives) was 83%, while the sensitivity (true positive rate) was 86%. Overall, the classifier performed well and the few dead seedlings present in the scene were excluded during the thresholding stages. However,

the process was sensitive to weeds and appeared to rely strongly on the contrast resulting from shadows cast by the taller seedlings.

Training of the template matching algorithm from the sample images was straightforward and the training images produced a template with low ambiguity. Comparison of different templates showed that the red channel was best, producing a higher correlation coefficient with new training samples. The template produced by this channel had a higher contrast between seedlings, surrounding vegetation, and the ground. A larger window size was also favoured. The seedlings averaged 20 - 25 cm diameter but the optimum window size was close to 60 cm. The template showed that the larger window size captured the effects of shadow on the South East side of the seedlings and adjacent ground. The template-matching output estimated the location of the top of each seedling. The results of the template applied to a new area not used to train the algorithm are shown in Figure 15.

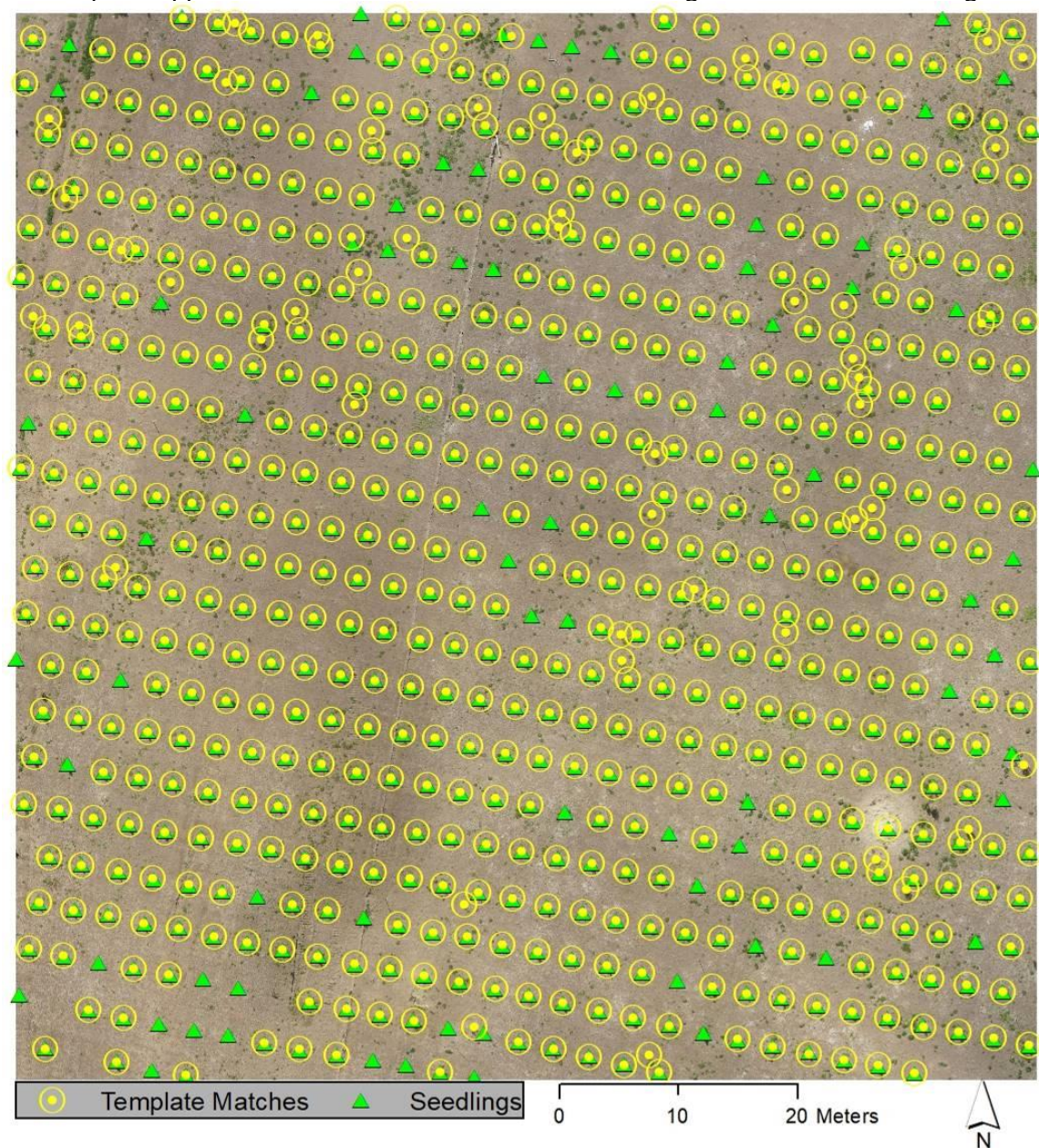


Figure 15: Results of template matching algorithm for detecting seedlings.

The classifier identified 619 seedlings, whereas the area was known to contain 642 seedlings. A correlation coefficient threshold of 0.775 appeared to produce a good balance between false negatives and positives. Higher coefficients reduced the detection of taller weeds as seedlings but increased the number of smaller seedlings missed by the

algorithm. The final classification produced 50 false positives, nearly all from tall, green weeds. At this threshold, a total of 73 seedlings were missed and these were almost all seedlings that were considerably smaller than the average for the site. The sensitivity was 89%, while the precision was 92%. These results were obtained by testing on a relatively large area but the results still surpassed the usefulness and accuracy of the OBIA classifier. The template matching approach appeared to benefit from the shadow and shape of the seedlings but the results excluded the few dead and missing seedlings present in both the training and test scenes owing to the low contrast between the ground and the red, senescing needles as well as the smaller shadow cast by these seedlings.

Applying the template to the heavily weed infested area produced poor results (not shown). This was due to the very dense vegetation that obscured both the seedlings and the shadow-related elements in the scene. Interestingly, the classifier suffered mostly from false positives from tall weeds, with many of the seedlings being identified. Had multispectral data been available, the strong contrast between the flowering weeds and the pines may have been useful in a revised classification aimed at reducing the false positive rate.

Discussion and conclusions

Overall, the results demonstrated that seedlings could be detected with a high level of accuracy across this site using only RGB imagery. Both the OBIA and template matching approaches produced accurate classifications, with the template matching algorithm producing a better compromise between false positives and false negatives. Both approaches benefitted substantially from the shadows cast by the taller seedlings and the contrast between the North West and South East portions of the seedlings. The shape and colour also assisted both classifications. The few dead seedlings in the scenes usually had red needles and showed less contrast and smaller area cast in shadow. Both classifications were capable of excluding these dead seedlings but the overall number available for testing was low and the classifiers may not have performed as well on examples with higher contrast or only partially dead foliage. Nearly all false positives resulted from taller weeds and the results from the heavily weed-infested site confirmed that high prevalence of weeds confuses the classification.

The demonstrated approaches are unlikely to perform as well on sites with a high level of weeds and the importance of shadows suggested that elevation of the vegetation within the scene was useful for classification. This suggests that the use of multispectral imagery and the dense matching point clouds from RGB imagery might be useful for classification. Multispectral imagery collected by Scion at other sites containing seedlings > 2 years old showed higher contrast between conifer seedlings and weed species using the red edge and near-infrared channels. However, the low resolution of current multispectral sensors made it impractical to collect data for the much smaller seedlings. Data from higher flights showed that the small seedlings became hard to detect at lower resolutions. This is important because the early assessment of mortality and stocking at e.g. 8 months allows forest managers to correct these issues during the next planting season. The advent of higher resolution multispectral camera is likely to overcome these issues and would allow the classifiers to be further refined to exclude weeds species. This study did not examine the use of synthetic point clouds or DSMs, but it may be possible to use values from a DSM produced by Pix4D or other image-matching software in place of the shadows that formed a proxy for vegetation height. Overall, the use of UAV-derived RGB imagery appeared to show promise for post-planting assessment but further testing across a broader range of sites, and potentially utilising newer multispectral sensors may validate and improve the practicality of this approach.

Post-harvest Waste Assessment

Background

Coarse woody debris (CWD) plays an important role within forests. This dead wood provides a long-term source of organic matter and nutrients to the forest soil (Karjalainen & Kuuluvainen, 2002; Siitonen, 2001; Yan, Wang, & Huang, 2006) and is a critical habitat for the maintenance of biodiversity (Bütler & Schlaepfer, 2004; Mielikäinen & Hynynen, 2003). The quantity of CWD also affects carbon dynamics (Bütler & Schlaepfer, 2004; Ståhl, Ringvall, & Fridman, 2001) and fire risk (Brown, Reinhardt, & Kramer, 2003). Consequently, information about the spatial distribution of CWD provides useful insight into soil nutrition, species distribution, biodiversity and biogeochemical cycles in forest ecosystems (Jia-bing, De-xin, Shi-jie, Mi, & Chang-jie, 2005).

CWD inventories have traditionally been undertaken using ground-based field surveys. Several unbiased methods for sampling CWD are available that include fixed area sampling, line intersect sampling, planar intersect sampling and transect relascope sampling (Jordan, Ducey, & Gove, 2004). Field campaigns to locate and characterise logs often need to be extensive as CWD is usually distributed in a random pattern that is not spatially contiguous. Consequently, field surveys are often expensive, labour intensive and difficult in remote areas or regions with broken or steep terrain (Bütler & Schlaepfer, 2004). The line intersect method (LIM) (Van Wagner, 1968, 1982) is commonly used in New Zealand to assess waste left on site and to ensure logging contractors have reached target values for recovery of merchantable timber (Warren & Olsen, 1964). The accuracy of the LIM method can be negatively impacted by violations of the assumption that pieces are randomly orientated, as might be encountered on wind-damaged areas (Bell, Kerr, McNickle, & Woollons, 1996). The accuracy of the LIM waste assessment also benefits from increased total transect length but the degree of improvement depends on site characteristics and can increase the cost of sampling using traditional field-based methods (Pickford & Hazard, 1978; Warren & Olsen, 1964).

Remote sensing methods such as manual aerial photo interpretation, manual or automatic interpretation of satellite images, and ocular estimation from aeroplanes or helicopters are used in the estimation phase to more effectively allocate sample plots (Ståhl et al., 2001). Research describing the use of remote sensing to directly estimate CWD is relatively sparse and most studies have used data collected from manned aircraft. Following a severe fire in Yellowstone Park, 1 m aerial imagery with four bands was used to map CWD in streams but proved to be relatively inaccurate (Marcus, Marston, Colvard, & Gray, 2002). Similarly, fused airborne Synthetic Aperture Radar (AirSAR) and optical Airborne Visible/Infrared Imaging Spectrometer (AVIRIS) was of limited use in detecting CWD, within this study area (S. Huang, Crabtree, Potter, & Gross, 2009). CWD was successfully mapped within Yellowstone Park, with an accuracy of 83%, using 1 m hyperspectral imagery (Marcus, Legleiter, Aspinall, Boardman, & Crabtree, 2003). In Gatineau Park, Québec, Pasher and King (2009) were able to accurately map 94% of dead wood objects using 20 cm multispectral imagery.

ALS data has been found to be moderately useful in the detection of CWD. Within the lodgepole pine and spruce/fir stands of Montana in the US, ALS was used to accurately describe the total fuel load which was mostly composed of CWD (Seielstad & Queen, 2003). Research undertaken in Koli National Park in eastern Finland (Pesonen, Maltamo, Eerikäinen, & Packalèn, 2008) showed that a model constructed using intensity data and height percentiles from ALS data was moderately accurate at predicting CWD (adjusted $R^2 = 0.61$; RMSE of 51.6%). Blanchard et al. (2011), investigated the utility of LiDAR at delineating downed logs in disturbed forest landscape in Lake Tahoe National Park,

California. Using an OBIA framework, 73% of downed log objects were successfully delineated and classified from LiDAR-derived metrics (Blanchard et al., 2011).

Although little research has investigated the utility of UAVs for detecting CWD, this could provide a promising avenue given the higher spatial resolution of the data and the relatively low cost of flying moderate sized areas. Fallen trees within a deciduous forest in eastern Japan were surveyed using high resolution aerial photographs (0.5-1.0 cm per pixel) acquired from a UAV (Inoue et al., 2014). This research was able to identify 80% to 90% of fallen trees that were >30 cm in diameter or >10 m in length but missed many that were narrower or shorter. Within a recently harvested plantation, Bryson and Sukkarieh (2016) used high-resolution colour imagery data (2 mm) collected from a UAV to characterise CWD through digital annotation. The method was successful and showed a very close correspondence ($R^2 = 0.99$) between estimated and measured volumes of CWD (Bryson & Sukkarieh, 2016).

This study aimed to evaluate the usefulness of RGB imagery acquired from a UAV as a means of assessing post-harvest waste. The method sought to replicate the results obtained using the LIM that is widely used in New Zealand and elsewhere as a means of estimating the volume of potentially merchantable timber left unrecovered. The study also sought to explore possible implications for future improvements in waste assessment methods based on availability and usefulness of UAV imagery.

Methods

This study focused on the feasibility of performing post-harvest waste assessment using RGB imagery acquired from a UAV. The primary objective was to compare measurements of CWD extracted from the imagery to measurements obtained using field-based LIM surveys. To accommodate this, the LIM field sampling protocol deviated from the sampling considerations required to achieve representative estimates of the residual material per hectare. The study design used an adaptation of the LIM layout but plots location and length were adjusted to include a larger number of pieces covering a range of sizes and the study was located on a site with moderate amounts of waste present.

In the field, eight plots were systematically located in a recently harvested site. The centre of each plot was located using a high-grade GPS, post-processed to centimetre accuracy. Two perpendicular transects were set out from each plot (Figure 16) with an orientation chosen to intersect visible waste elements. The total transect length was 345 m, with most transects measuring approximately 20 m. In some cases, transects were extended to a maximum of 27 m to include additional waste pieces. The line intersect method requires the definition of minimum piece size based on e.g. length and small end diameter (SED), and large end diameter (LED) to determine if waste pieces should be included in measurements. For this study, all waste pieces with length > 1 m and SED > 10 cm were measured. The cross-sectional diameter at the point the transect line intersected each piece was measured using callipers or a DBH tape. In addition to this, the SED, LED and length between these points were also recorded and marked with blue paint. Excessive sweep, rot, and other defects on identified waste pieces were noted to assess whether these could be detected from the imagery.

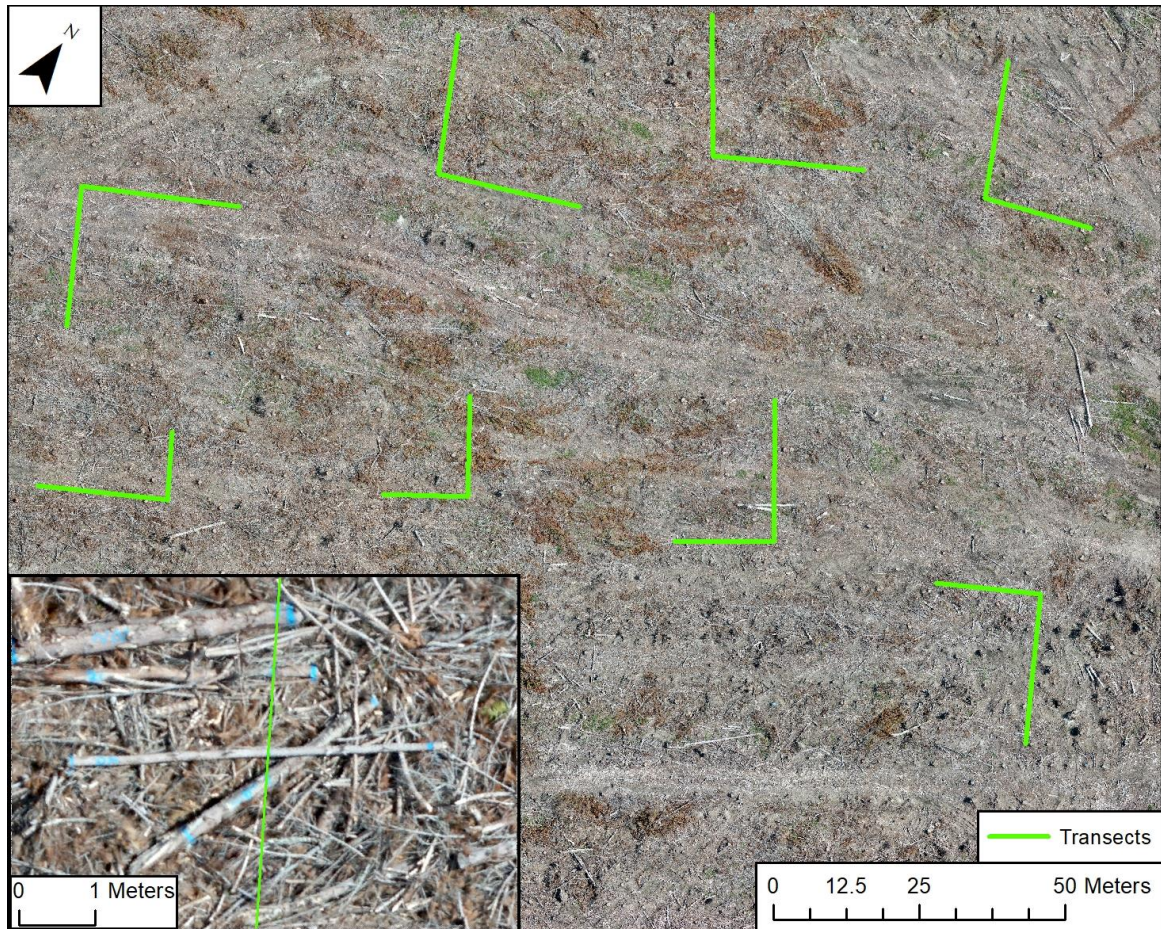


Figure 16: Study site and layout for post-harvest waste assessment based on the line intersect method. Blue paint indicated the locations where field measurements were collected.

A summary of the key characteristics for the imagery collected is shown in Table 9. Images were processed using Pix4D mapper with ground-control points inserted before refining the final orthomosaic to ensure accurate geo-rectification. The transect lines were located in the imagery using a GIS. Waste pieces intercepted by these lines were identified and annotated by locating the painted marks on the pieces and defining a polyline in the GIS. This process was carried out without reference to the field measurements. The final annotated layer marked the length, SED, LED, and cross-sectional diameter at the point of field measurement (identifiable from the painted marks in the imagery).

Table 9: Description of key characteristics for datasets collected over recent harvest site.

Data characteristics	Values
Imagery extent (ha)	6.4 ha
Ground sample distance (cm/pixel)	0.7
Flight altitude	30 m
Number of images	701
Image channels	RGB
Ground control	Yes (8)
Forward / side overlap (%)	88 / 90

The field measurements were graphically compared to the annotated measurements obtained from the imagery. Both sets of measurements were then used to calculate the approximate volume of each piece as a conical frustum according to the equation:

$$V = \frac{1}{3}\pi L \left(\left(\frac{LED}{2} \right)^2 + \left(\frac{LED * SED}{4} \right) + \left(\frac{SED}{2} \right)^2 \right)$$

Where L is the piece length, SED is the small end diameter and LED the large end diameter. This volume of waste per unit area was then computed using the line intersect equation of Van Wagner (1968, 1982):

$$V = \left(\frac{\pi^2}{8L} \right) \sum D^2$$

Where L is the length of the transect line along which the pieces lie and D is the cross-sectional diameter at the point of intersection on this line. The estimates of waste and individual piece volumes from annotated imagery and field measurement were compared. Finally, an assessment was conducted to determine if defects could be located on larger pieces that may have been correctly left as waste because of e.g. rot or excessive sweep noted by the harvesting crews.

Results

In total, 60 waste pieces were identified and measured covering a range of lengths and diameters (Table 10). The annotated measurements extracted from the orthomosaic agreed well with field measurements at nearly all points. The maximum difference of 14 cm occurred measuring the length of a 9 m piece with moderate sweep (Table 10). The average difference between field and imagery measurements was generally low with length measurements showing the highest error (Table 10). This was usually due to sweep or difficulty identifying ends that were covered by slash or other debris.

Table 10: Summary statistics for measured waste pieces.

	SED		Intersect		LED		Length	
	Field	Imagery	Field	Imagery	Field	Imagery	Field	Imagery
Mean (cm)	17	16	19	18	20	21	339	333
Std. Dev (cm)	7	7	8	7	8	8	173	173
Min (cm)	10	7	11	9	11	11	115	112
Max (cm)	47	43	50	54	55	58	920	934
Absolute Mean difference (cm)	2.3		1.7		2		9.9	

Some artefacts were observed in the final orthomosaic (Figure 17, Top); however, none of the identified transects ran through these areas. These artefacts were likely caused by poor matching of images covering these locations but the affected regions were small and the remaining orthomosaic showed very high levels of detail across the site (Figure 17, bottom).



Figure 17: Example of image ghosting from poor matching during orthomosaic generation (top). The bottom panel shows the typical level of detail achieved across most of the site from imagery with a GSD of 0.7 cm/pixel.

The volume defined by a frustum of a cone was computed using the field and imagery measurements of length, SED, and LED. The volumes computed in this way agreed well for all 60 pieces and a regression between these values showed strong agreement ($R^2 = 0.95$) with an intercept of 0 and a slope nearly equal to 1 showing strong agreement across the range (Figure 18). The volume of pieces ranged from 0.03 m³ to 0.8 m³ but most pieces were quite small (mean = 0.12 m³), as could be expected in a waste assessment. The volume and dimensions of the largest piece were well estimated from the imagery; however, field inspection could identify that this piece was left due to extensive rot. This was not immediately evident from the UAV imagery. The volume per hectare from the field estimates was 85.6 m³/ha while the estimate from the image-based measurements was 84.4 m³/ha. Although these estimates agreed well, the deliberately biased sampling strategy made these values considerably higher than might be expected from a random sample. The process of annotating imagery was straightforward and could be accomplished efficiently using nearly any GIS software.

The results from inspection of identified pieces for defects produced mixed results. The key limitation of the imagery-based approach was the inability to identify rot and difficulty identifying and measuring pieces hidden by other slash and debris. However, the imagery could be used to easily trace out pieces with significant sweep, and it would have been feasible to compute the actual sweep from the annotations as a verification of the harvest crew's assessment. Broken or shattered pieces occasionally posed a challenge for SED and LED measurements but were rarely an issue when focusing only on the diameter at the point of intercept.

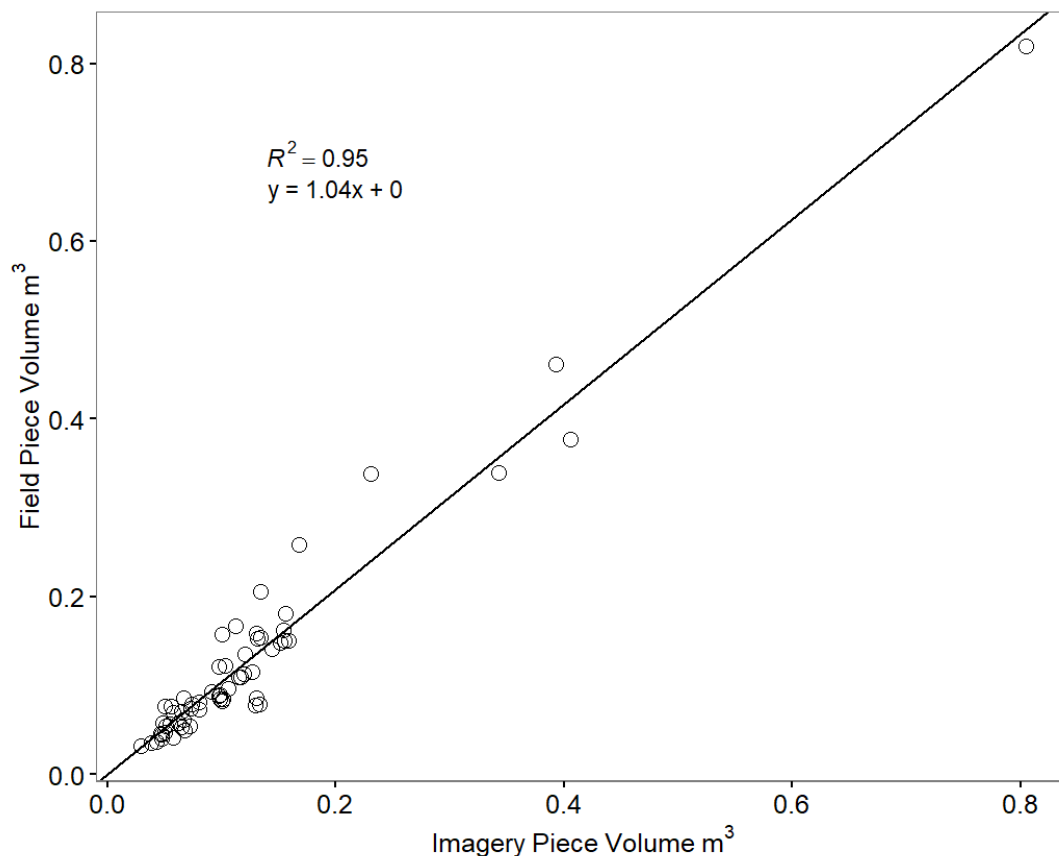


Figure 18: Regression of volume estimates for 60 waste pieces calculated using field measurements and measurements extracted from digital annotation of UAV imagery.

Discussion and conclusions

The primary objective of this study was to evaluate the utility of RGB imagery for post-harvest waste assessment. Digital annotations extracted from the geo-rectified imagery

showed excellent agreement with measurements obtained in the field. The study relied on replicating the line intersect sampling approach as this method is widely used in New Zealand to conduct post-harvest waste assessment. While the imagery provided a very similar estimate of residual volume, several key advantages were noted when using the RGB imagery. LIM sampling is constrained by the need to physically move around the site to locate and measure transects. This may constrain the number, location and total length of transects achievable and this may impact the error of the estimates (Van Wagner, 1968, 1982). The image-based approach was much less constrained and it would have been feasible to place transects anywhere where the imagery was free from artefacts, and potentially long transect lines could have been marked in any direction. The process of measuring pieces was straightforward and most GIS software includes template tools to assess the size of objects – allowing small, in-eligible pieces to be rapidly excluded. Another advantage of the image-based approach was the ability to easily identify the general orientation of pieces across the site. This is important because the non-random orientation of pieces has been shown to induce serious errors in LIM-based estimates of waste volume (Bell et al., 1996). One approach to overcome non-random orientation is to arrange transects as equilateral triangles. While this works well it is often costly and hard when done in the field (Bell et al., 1996). The image-based approach could help to both identify sites with non-random orientation of pieces and to implement transect layouts best suited to minimising error in the estimates derived from these sites in a cost-effective manner.

One key disadvantage of the image-based approach was the inability to identify rot in the imagery. This might lead to an overestimation of waste when these pieces are erroneously included in the survey. It was also difficult to measure pieces where slash obstructed clear views; however, this must be weighed against the potential advantages such as the ability to survey longer transects, to accurately measure sweep, and to improve the layout of plots by e.g. sampling hard-to-reach areas. This study also lacked imagery covering steep sites. In theory, the dense matching point cloud could be used to provide an accurate estimate of the slope to correct any measurements but this was not tested and other factors such as long shadows or poor illumination on steep sites might pose challenges to image-based approaches. Future work might explore the method applied to a wider range of areas and sites. A key area for further investigation should be the use of the imagery and dense matching point clouds to automatically identify debris, potentially using OBIA. Successful identification of larger pieces from these data could allow assessment of waste across most or all of a recently harvested site.

Conclusions

Remote sensing is widely used in New Zealand's forestry sector. UAVs offer new opportunities to collect these data but the cost efficacy and potential applications have not been broadly explored. A survey of data providers suggested that LiDAR is increasingly sought by forestry companies but UAVs are not yet capable of delivering routine LiDAR products. Instead, UAVs currently fill a niche role in the provision of RGB and multispectral imagery. UAVs were most cost-effective for areas up to 100 ha and offered rapid capture of very high resolution imagery products. These data showed promise for a range of potential applications within the sector. This study demonstrated the potential for autonomous mapping of cutover areas using a customised UAV and detection and mapping of wind-thrown forest using fixed wing craft that can capture larger areas. Operational applications such as post-harvest waste assessment also appeared promising, with methods based on imagery showing strong agreement with field-based assessments. Tasks such as post-planting survival assessment were more challenging but advances in sensor capabilities are likely to overcome the identified limitations. As sensors and craft develop it is expected that UAVs and the data they can provide will play an increasing role in New Zealand forestry.

Acknowledgements

This project was funded by the Forest Owners Association and the Forest Growers Levy Trust with additional funding provided from Scion's core funding. The authors would like to thank: Michael Wilson, Marika Fritzsche, and Ian Hinton of Timberlands Ltd. for providing forest access, study locations, and assistance with data collection; Michael Baker of Hancock Forest Management for useful ideas and feedback; Mark Forward of Nelson Forests and Kevan Buck of Buck Forestry for imagery and data in the Nelson region; Rayonier for forest access and data at Bottle Lake Forest park; The many service providers who took the time to provide survey information; and the dedicated field technicians who collected data at the different trial site locations.

References

- Abburu, S., & Golla, S. B. (2015). Satellite image classification methods and techniques: A review. *International journal of computer applications*, 119(8).
- Aguilar, M. A., Saldaña, M. d. M., & Aguilar, F. J. (2013). Assessing geometric accuracy of the orthorectification process from GeoEye-1 and WorldView-2 panchromatic images. *International Journal of Applied Earth Observation and Geoinformation*, 21, 427-435. doi:http://dx.doi.org/10.1016/j.jag.2012.06.004
- Ahern, F. (1988). The effects of bark beetle stress on the foliar spectral reflectance of lodgepole pine. *International Journal of Remote Sensing*, 9(9), 1451-1468.
- Allen, C. D., Macalady, A. K., Chenchouni, H., Bachelet, D., McDowell, N., Vennetier, M., . . . Hogg, E. T. (2010). A global overview of drought and heat-induced tree mortality reveals emerging climate change risks for forests. *Forest ecology and management*, 259(4), 660-684.
- Anderson, K., & Gaston, K. J. (2013). Lightweight unmanned aerial vehicles will revolutionize spatial ecology. *Frontiers in Ecology and the Environment*, 11(3), 138-146. doi:10.1890/120150
- Bastin, J.-F., Berrahmouni, N., Grainger, A., Maniatis, D., Mollicone, D., Moore, R., . . . Castro, R. (2017). The extent of forest in dryland biomes. *Science*, 356, 635-638. doi:10.1126/science.aam6527
- Bell, G., Kerr, A., McNickle, D., & Woollons, R. (1996). Accuracy of the line intersect method of post-logging sampling under orientation bias. *Forest ecology and management*, 84, 23-28. doi:10.1016/0378-1127(96)03773-5
- Blanchard, S. D., Jakubowski, M. K., & Kelly, M. (2011). Object-Based Image Analysis of Downed Logs in Disturbed Forested Landscapes Using Lidar. *Remote Sensing*, 3, 2420-2439. doi:10.3390/rs3112420
- Blaschke, T. (2010). Object based image analysis for remote sensing. *ISPRS Journal of Photogrammetry and Remote Sensing*, 65, 2-16. doi:10.1016/j.isprsjprs.2009.06.004
- Boutet, J. C., & Weishampel, J. F. (2003). Spatial pattern analysis of pre- and post-hurricane forest canopy structure in North Carolina, USA. *Landscape Ecology*, 18, 553-559. doi:10.1023/A:1026058312853
- Briechele, K., & Hanebeck, U. D. (2001). *Template matching using fast normalized cross correlation*.
- Brown, J. K., Reinhardt, E. D., & Kramer, K. A. (2003). *Coarse woody debris: managing benefits and fire hazard in the recovering forest*: US Department of Agriculture, Forest Service, Rocky Mountain Research Station.
- Bryson, M., & Sukkarieh, S. (2016). Deployment and integration of cost-effective, high spatial resolution, remotely sensed data for the Australian forest industry. *FWPA report*.
- Bulinski, J., & McArthur, C. (1999). An experimental field study of the effects of mammalian herbivore damage on Eucalyptus nitens seedlings. *Forest ecology and management*, 113(2), 241-249. doi:http://dx.doi.org/10.1016/S0378-1127(98)00430-7
- Bütler, R., & Schlaepfer, R. (2004). Spruce snag quantification by coupling colour infrared aerial photos and a GIS. *Forest ecology and management*, 195(3), 325-339.
- Chehata, N., Orny, C., Boukir, S., Guyon, D., & Wigneron, J. P. (2014). Object-based change detection in wind storm-damaged forest using high-resolution multispectral images. *International Journal of Remote Sensing*, 35(13), 4758-4777. doi:10.1080/01431161.2014.930199
- Coops, N. C., Johnson, M., Wulder, M. A., & White, J. C. (2006). Assessment of QuickBird high spatial resolution imagery to detect red attack damage due to mountain pine beetle infestation. *Remote sensing of environment*, 103(1), 67-80.
- Curran, P. J., Dungan, J. L., & Gholz, H. L. (1990). Exploring the Relationship between Reflectance Red Edge and Chlorophyll Content in Slash Pine. *Tree Physiology*, 7(1-4), 33-48.
- Dennison, P. E., Brunelle, A. R., & Carter, V. A. (2010). Assessing canopy mortality during a mountain pine beetle outbreak using GeoEye-1 high spatial resolution satellite data. *Remote sensing of environment*, 114(11), 2431-2435.
- Duan, F., Wan, Y., & Deng, L. (2017). A Novel Approach for Coarse-to-Fine Windthrown Tree Extraction Based on Unmanned Aerial Vehicle Images. *Remote Sensing*, 9(4), 306. doi:10.3390/rs9040306
- Edburg, S. L., Hicke, J. A., Brooks, P. D., Pendall, E. G., Ewers, B. E., Norton, U., . . . Meddens, A. J. (2012). Cascading impacts of bark beetle-caused tree mortality on coupled

- biogeophysical and biogeochemical processes. *Frontiers in Ecology and the Environment*, 10(8), 416-424.
- FOA. (2016). *Facts and Figures 2015/2016*. Retrieved from Wellington:
- Franklin, S., Wulder, M., Skakun, R., & Carroll, A. (2003). Mountain pine beetle red-attack forest damage classification using stratified Landsat TM data in British Columbia, Canada. *Photogrammetric Engineering & Remote Sensing*, 69(3), 283-288.
- Fransson, J. E. S., Magnusson, M., Folkesson, K., Hallberg, B., Sandberg, G., Smith-Jonforsen, G., . . . Ulander, L. M. H. (2007, 23-28 July 2007). *Mapping of wind-thrown forests using VHF/UHF SAR images*. Paper presented at the 2007 IEEE International Geoscience and Remote Sensing Symposium.
- Fraser, R., & Latifovic, R. (2005). Mapping insect-induced tree defoliation and mortality using coarse spatial resolution satellite imagery. *International Journal of Remote Sensing*, 26(1), 193-200.
- Gardiner, B., Schuck, A. R. T., Schelhaas, M.-J., Orazio, C., Blennow, K., & Nicoll, B. (2013). *Living with storm damage to forests*: European Forest Institute.
- Gartner, M. H., Veblen, T. T., Leyk, S., & Wessman, C. A. (2015). Detection of mountain pine beetle-killed ponderosa pine in a heterogeneous landscape using high-resolution aerial imagery. *International Journal of Remote Sensing*, 36(21), 5353-5372.
- GlobalForestWatch. (2017). Global Forest Watch. Retrieved from www.globalforestwatch.org/
- Grenzdörffer, G. J., Engel, A., & Teichert, B. (2008). The photogrammetric potential of low-cost UAVs in forestry and agriculture. *The International Archives of the Photogrammetry, Remote Sensing and Spatial Information Sciences*, 31, 1207-1214.
- Guo, Q., Kelly, M., Gong, P., & Liu, D. (2007). An object-based classification approach in mapping tree mortality using high spatial resolution imagery. *GIScience & Remote Sensing*, 44(1), 24-47.
- Hansen, M. C., Potapov, P. V., Moore, J. R., Hancher, M., Turubanova, S. A., Tyukavina, A., . . . Townshend, J. R. G. (2013). High-Resolution Global Maps of 21st-Century Forest Cover Change. *Science*, 342, 850-853. doi:10.1126/science.1244693
- Hansen, M. C., Stehman, S. V., & Potapov, P. V. (2010). Quantification of global gross forest cover loss. *Proceedings of the National Academy of Sciences*, 107, 8650-8655. doi:10.1073/pnas.0912668107
- Hérissé, B., Hamel, T., Mahony, R., & Russotto, F.-X. (2010). A terrain-following control approach for a VTOL Unmanned Aerial Vehicle using average optical flow. *Autonomous Robots*, 29(3), 381-399. doi:10.1007/s10514-010-9208-x
- Hérissé, B., Russotto, F.-X., Hamel, T., & Mahony, R. (2008, 2008). *Hovering flight and vertical landing control of a VTOL unmanned aerial vehicle using optical flow*.
- Herrmann, K., Rock, B. N., Ammer, U., & Paley, H. N. (1988). Preliminary assessment of airborne imaging spectrometer and airborne thematic mapper data acquired for forest decline areas in the Federal Republic of Germany. *Remote sensing of environment*, 24(1), 129-149.
- Hicke, J. A., & Logan, J. (2009). Mapping whitebark pine mortality caused by a mountain pine beetle outbreak with high spatial resolution satellite imagery. *International Journal of Remote Sensing*, 30(17), 4427-4441.
- Holmgren, P., & Thuresson, T. (1998). Satellite remote sensing for forestry planning—A review. *Scandinavian Journal of Forest Research*, 13(1-4), 90-110. doi:10.1080/02827589809382966
- Honkavaara, E., Litkey, P., & Nurminen, K. (2013). Automatic Storm Damage Detection in Forests Using High-Altitude Photogrammetric Imagery. *Remote Sensing*, 5(3), 1405.
- Horcher, A., & Visser, R. J. (2004). Unmanned aerial vehicles: applications for natural resource management and monitoring. *Proceedings of the Council on Forest Engineering Proceedings*.
- Huang, C., Davis, L. S., & Townshend, J. R. G. (2002). An assessment of support vector machines for land cover classification. *International Journal of Remote Sensing*, 23(4), 725-749. doi:10.1080/01431160110040323
- Huang, C. Y., & Anderegg, W. R. (2012). Large drought-induced aboveground live biomass losses in southern rocky mountain aspen forests. *Global Change Biology*, 18(3), 1016-1027.
- Huang, S., Crabtree, R. L., Potter, C., & Gross, P. (2009). Estimating the quantity and quality of coarse woody debris in Yellowstone post-fire forest ecosystem from fusion of SAR and optical data. *Remote sensing of environment*, 113(9), 1926-1938.
- Hunt, D. (2016). An unmanned aerial vehicle for autonomous forestry cutover edge survey.
- Inoue, T., Nagai, S., Yamashita, S., Fadaei, H., Ishii, R., Okabe, K., . . . Suzuki, R. (2014). Unmanned aerial survey of fallen trees in a deciduous broadleaved forest in eastern Japan. *PloS one*, 9(10), e109881.

- Jia-bing, W., De-xin, G., Shi-jie, H., Mi, Z., & Chang-jie, J. (2005). Ecological functions of coarse woody debris in forest ecosystem. *Journal of Forestry Research*, 16(3), 247-252.
- Jones, G. P., Pearlstine, L. G., & Percival, H. F. (2006). An Assessment of Small Unmanned Aerial Vehicles for Wildlife Research. *Wildlife Society Bulletin (1973-2006)*, 34(3), 750-758.
- Jordan, G., Ducey, M. J., & Gove, J. H. (2004). Comparing line-intersect, fixed-area, and point relascope sampling for dead and downed coarse woody material in a managed northern hardwood forest. *Canadian Journal of Forest Research*, 34(8), 1766-1775.
- Karjalainen, L., & Kuuluvainen, T. (2002). Amount and diversity of coarse woody debris within a boreal forest landscape dominated by *Pinus sylvestris* in Vienansalo wilderness, eastern Fennoscandia. *Silva Fennica*, 36(1), 147-167.
- Keenan, R. J., Reams, G. A., Achard, F., de Freitas, J. V., Grainger, A., & Lindquist, E. (2015). Dynamics of global forest area: Results from the FAO Global Forest Resources Assessment 2015. *Forest ecology and management*, 352, 9-20. doi:10.1016/j.foreco.2015.06.014
- Kennedy, R. E., Yang, Z., & Cohen, W. B. (2010). Detecting trends in forest disturbance and recovery using yearly Landsat time series: 1. LandTrendr — Temporal segmentation algorithms. *Remote sensing of environment*, 114, 2897-2910. doi:10.1016/j.rse.2010.07.008
- LandsatFACT. (2017). LandsatFACT. Retrieved from <https://nemas.unca.edu/landsatfact>
- Leckie, D., Teillet, P., Fedosejevs, G., & Ostaff, D. (1988). Reflectance characteristics of cumulative defoliation of balsam fir. *Canadian Journal of Forest Research*, 18(8), 1008-1016.
- Liu, X., Zhang, Z., Peterson, J., & Chandra, S. (2007). LiDAR-Derived High Quality Ground Control Information and DEM for Image Orthorectification. *Geoinformatica*, 11(1), 37-53. doi:10.1007/s10707-006-0005-9
- Macomber, S. A., & Woodcock, C. E. (1994). Mapping and monitoring conifer mortality using remote sensing in the Lake Tahoe Basin. *Remote sensing of environment*, 50(3), 255-266.
- Mahalanobis, P. C. (1936). *On the generalised distance in statistics*. Paper presented at the Proceedings National Institute of Science, India.
- Marcus, W. A., Legleiter, C. J., Aspinall, R. J., Boardman, J. W., & Crabtree, R. L. (2003). High spatial resolution hyperspectral mapping of in-stream habitats, depths, and woody debris in mountain streams. *Geomorphology*, 55(1), 363-380.
- Marcus, W. A., Marston, R. A., Colvard, C. R., & Gray, R. D. (2002). Mapping the spatial and temporal distributions of woody debris in streams of the Greater Yellowstone Ecosystem, USA. *Geomorphology*, 44(3), 323-335.
- Martin, T. J., & Ogden, J. (2006). Wind damage and response in New Zealand forests: a review. *New Zealand Journal of Ecology*, 30(3), 295-310.
- Mason, E. G., South, D. B., & Weizhong, Z. (1996). Performance of *Pinus radiata* in relation to seedling grade, weed control, and soil cultivation in the central North Island of New Zealand. *New Zealand Journal of Forestry Science*, 26(1/2), 173-183.
- Meddens, A. J., Hicke, J. A., & Vierling, L. A. (2011). Evaluating the potential of multispectral imagery to map multiple stages of tree mortality. *Remote sensing of environment*, 115(7), 1632-1642.
- Meigs, G. W., Kennedy, R. E., & Cohen, W. B. (2011). A Landsat time series approach to characterize bark beetle and defoliator impacts on tree mortality and surface fuels in conifer forests. *Remote sensing of environment*, 115(12), 3707-3718.
- Mielikäinen, K., & Hynynen, J. (2003). Silvicultural management in maintaining biodiversity and resistance of forests in Europe–boreal zone: case Finland. *Journal of environmental management*, 67(1), 47-54.
- Moore, J. R., Manley, B., & Park, D. (2011). *Quantification and Management of the Risk of Wind Damage to New Zealand's Planted Forests*. Wellington: Ministry of Agriculture and Forestry.
- Moore, J. R., Manley, B. R., Park, D., & Scarrott, C. J. (2013). Quantification of wind damage to New Zealand's planted forests. *Forestry: An International Journal of Forest Research*, 86, 173-183. doi:10.1093/forestry/cps076
- Moore, J. R., & Somerville, A. (1998). Assessing the risk of wind damage to plantation forests in New Zealand. *New Zealand Forestry*, 43(1), 25-29.
- Morgenroth, J., & Visser, R. (2013). Uptake and barriers to the use of geospatial technologies in forest management. *New Zealand Journal of Forestry Science*, 43, 16. doi:10.1186/1179-5395-43-16

- Mountrakis, G., Im, J., & Ogole, C. (2011). Support vector machines in remote sensing: A review. *ISPRS Journal of Photogrammetry and Remote Sensing*, 66(3), 247-259. doi:<http://dx.doi.org/10.1016/j.isprsjprs.2010.11.001>
- MPI. (2016). *National Exotic Forest Description*. Retrieved from Wellington:
- Myers, R. K., & van Lear, D. H. (1998). Hurricane-fire interactions in coastal forests of the south: a review and hypothesis. *Forest ecology and management*, 103, 265-276. doi:10.1016/S0378-1127(97)00223-5
- Ogden, J. (1988). Forest dynamics and stand-level dieback in New Zealand's Nothofagus forests. *GeoJournal*, 17, 225-230. doi:10.1007/BF02432926
- Pajares, G. (2015). Overview and Current Status of Remote Sensing Applications Based on Unmanned Aerial Vehicles (UAVs). *Photogrammetric Engineering & Remote Sensing*, 81(4), 281-330. doi:10.14358/PERS.81.4.281
- Pal, M., & Mather, P. M. (2005). Support vector machines for classification in remote sensing. *International Journal of Remote Sensing*, 26(5), 1007-1011. doi:10.1080/01431160512331314083
- Pasher, J., & King, D. J. (2009). Mapping dead wood distribution in a temperate hardwood forest using high resolution airborne imagery. *Forest ecology and management*, 258(7), 1536-1548.
- Pesonen, A., Maltamo, M., Eerikäinen, K., & Packalèn, P. (2008). Airborne laser scanning-based prediction of coarse woody debris volumes in a conservation area. *Forest ecology and management*, 255(8), 3288-3296.
- Pickford, S. G., & Hazard, J. W. (1978). Simulation Studies on Line Intersect Sampling of Forest Residue. *Forest Science*, 24(4), 469-483.
- Puliti, S., Ørka, H. O., Gobakken, T., & Næsset, E. (2015). Inventory of Small Forest Areas Using an Unmanned Aerial System. *Remote Sensing*, 7, 9632-9654. doi:10.3390/rs70809632
- Rathinam, S., Almeida, P., Kim, Z., Jackson, S., Tinka, A., Grossman, W., & Sengupta, R. (2007, 9-13 July 2007). *Autonomous Searching and Tracking of a River using an UAV*. Paper presented at the 2007 American Control Conference.
- Reglinski, T., & Dick, M. (2005). Biocontrol of forest nursery pathogens. *New Zealand Journal of Forestry*, 50(3), 19.
- Rock, B., Hoshizaki, T., & Miller, J. (1988). Comparison of in situ and airborne spectral measurements of the blue shift associated with forest decline. *Remote sensing of environment*, 24(1), 109-127.
- Sader, S. A., Bertrand, M., & Wilson, E. H. (2003). Satellite Change Detection of Forest Harvest Patterns on an Industrial Forest Landscape. *Forest Science*, 49, 341-353.
- Sader, S. A., & Legaard, K. R. (2008). Inclusion of forest harvest legacies, forest type, and regeneration spatial patterns in updated forest maps: A comparison of mapping results. *Forest ecology and management*, 255, 3846-3856. doi:10.1016/j.foreco.2008.03.047
- Sarvaiya, J. N., Patnaik, S., & Bombaywala, S. (2009, 28-29 Dec. 2009). *Image Registration by Template Matching Using Normalized Cross-Correlation*. Paper presented at the 2009 International Conference on Advances in Computing, Control, and Telecommunication Technologies.
- Scilab. (2012). Scilab: Free and Open Source software for numerical computation. Retrieved from <http://www.scilab.org>
- Seielstad, C. A., & Queen, L. P. (2003). Using airborne laser altimetry to determine fuel models for estimating fire behavior. *Journal of Forestry*, 101(4), 10-15.
- Siitonen, J. (2001). Forest management, coarse woody debris and saproxylic organisms: Fennoscandian boreal forests as an example. *Ecological bulletins*, 11-41.
- Sims, D. A., & Gamon, J. A. (2002). Relationships between leaf pigment content and spectral reflectance across a wide range of species, leaf structures and developmental stages. *Remote sensing of environment*, 81(2), 337-354.
- Skakun, R. S., Wulder, M. A., & Franklin, S. E. (2003). Sensitivity of the thematic mapper enhanced wetness difference index to detect mountain pine beetle red-attack damage. *Remote sensing of environment*, 86(4), 433-443.
- Ståhl, G., Ringvall, A., & Fridman, J. (2001). Assessment of coarse woody debris: a methodological overview. *Ecological bulletins*, 57-70.
- Stone, C., Penman, T., & Turner, R. (2012). Managing drought-induced mortality in *Pinus radiata* plantations under climate change conditions: a local approach using digital camera data. *Forest ecology and management*, 265, 94-101.
- Szantoi, Z., Malone, S., Escobedo, F., Misas, O., Smith, S., & Dewitt, B. (2012). A tool for rapid post-hurricane urban tree debris estimates using high resolution aerial imagery.

- International Journal of Applied Earth Observation and Geoinformation*, 18, 548-556.
doi:10.1016/j.jag.2011.10.009
- Tang, L., & Shao, G. (2015). Drone remote sensing for forestry research and practices. *Journal of Forestry Research*, 26, 791-797. doi:10.1007/s11676-015-0088-y
- Toth, C., & Józków, G. (2016). Remote sensing platforms and sensors: A survey. *ISPRS Journal of Photogrammetry and Remote Sensing*, 115, 22-36.
doi:http://dx.doi.org/10.1016/j.isprsjprs.2015.10.004
- Toutin, T. (2004). Review article: Geometric processing of remote sensing images: models, algorithms and methods. *International Journal of Remote Sensing*, 25(10), 1893-1924.
doi:10.1080/0143116031000101611
- Tropek, R., Sedláček, O., Beck, J., Keil, P., Musilová, Z., Šimová, I., & Storch, D. (2014). Comment on "High-resolution global maps of 21st-century forest cover change". *Science*, 344, 981-981. doi:10.1126/science.1248753
- Ullman, S. (1979). The Interpretation of Structure from Motion. *Proceedings of the Royal Society of London. Series B. Biological Sciences*, 203(1153), 405-426. doi:10.1098/rspb.1979.0006
- Van Wagner, C. (1968). The line intersect method in forest fuel sampling. *Forest Science*, 14(1), 20-26.
- Van Wagner, C. (1982). *Practical aspects of the line intersect method* (Vol. 12). Chalk River, Canada: Petawawa National Forestry Institute.
- Villar-Salvador, P., Puértolas, J., Cuesta, B., Peñuelas, J. L., Uscola, M., Heredia-Guerrero, N., & Rey Benayas, J. M. (2012). Increase in size and nitrogen concentration enhances seedling survival in Mediterranean plantations. Insights from an ecophysiological conceptual model of plant survival. *New Forests*, 43(5), 755-770. doi:10.1007/s11056-012-9328-6
- Vollenweider, P., & Günthardt-Goerg, M. S. (2005). Diagnosis of abiotic and biotic stress factors using the visible symptoms in foliage. *Environmental Pollution*, 137(3), 455-465.
- Wallace, L., Musk, R., & Lucieer, A. (2014). An Assessment of the Repeatability of Automatic Forest Inventory Metrics Derived From UAV-Borne Laser Scanning Data. *IEEE Transactions on Geoscience and Remote Sensing*, 52, 7160-7169.
doi:10.1109/TGRS.2014.2308208
- Wang, F., & Xu, Y. J. (2010). Comparison of remote sensing change detection techniques for assessing hurricane damage to forests. *Environmental Monitoring and Assessment*, 162, 311-326. doi:10.1007/s10661-009-0798-8
- Wang, W., Qu, J. J., Hao, X., Liu, Y., & Stanturf, J. A. (2010). Post-hurricane forest damage assessment using satellite remote sensing. *Agricultural and Forest Meteorology*, 150, 122-132. doi:10.1016/j.agrformet.2009.09.009
- Warren, W. G., & Olsen, P. F. (1964). A Line Intersect Technique for Assessing Logging Waste. *Forest Science*, 10(3), 267-276.
- Watts, A. C., Ambrosia, V. G., & Hinkley, E. A. (2012). Unmanned Aircraft Systems in Remote Sensing and Scientific Research: Classification and Considerations of Use. *Remote Sensing*, 4(6), 1671.
- White, J., Coops, N., Hilker, T., Wulder, M., & Carroll, A. (2007). Detecting mountain pine beetle red attack damage with EO-1 Hyperion moisture indices. *International Journal of Remote Sensing*, 28(10), 2111-2121.
- White, J. C., Coops, N. C., Wulder, M. A., Vastaranta, M., Hilker, T., & Tompalski, P. (2016). Remote Sensing Technologies for Enhancing Forest Inventories: A Review. *Canadian Journal of Remote Sensing*, 42(5), 619-641. doi:10.1080/07038992.2016.1207484
- White, J. C., Wulder, M. A., Brooks, D., Reich, R., & Wheate, R. D. (2005). Detection of red attack stage mountain pine beetle infestation with high spatial resolution satellite imagery. *Remote sensing of environment*, 96(3), 340-351.
- White, J. C., Wulder, M. A., Hermosilla, T., Coops, N. C., & Hobart, G. W. (2017). A nationwide annual characterization of 25 years of forest disturbance and recovery for Canada using Landsat time series. *Remote sensing of environment*, 194, 303-321.
doi:10.1016/j.rse.2017.03.035
- Williams, A. P., Allen, C. D., Millar, C. I., Swetnam, T. W., Michaelsen, J., Still, C. J., & Leavitt, S. W. (2010). Forest responses to increasing aridity and warmth in the southwestern United States. *Proceedings of the National Academy of Sciences*, 107(50), 21289-21294.
- Wilson, E. H., & Sader, S. A. (2002). Detection of forest harvest type using multiple dates of Landsat TM imagery. *Remote sensing of environment*, 80, 385-396. doi:10.1016/S0034-4257(01)00318-2
- Wulder, M. A., Dymond, C. C., White, J. C., Leckie, D. G., & Carroll, A. L. (2006). Surveying mountain pine beetle damage of forests: A review of remote sensing opportunities. *Forest ecology and management*, 221(1), 27-41.

- Wulder, M. A., White, J. C., Coops, N. C., & Butson, C. R. (2008). Multi-temporal analysis of high spatial resolution imagery for disturbance monitoring. *Remote sensing of environment*, 112(6), 2729-2740.
- Yan, E., Wang, X., & Huang, J. (2006). Concept and classification of coarse woody debris in forest ecosystems. *Frontiers of Biology in China*, 1(1), 76-84.